

---

---

# Using Tactile Sensing to Inform Low-Cost, Force-Feedback Haptics

---

---

By

CHRISTOPHER WHITE



Department of Engineering Mathematics  
UNIVERSITY OF BRISTOL

A dissertation submitted to the University of Bristol in accordance with the requirements of the degree of MASTER OF ENGINEERING in the Faculty of Engineering.

APRIL 2023



## ABSTRACT

Optical tactile sensors have seen little use in providing haptic feedback to a remote operator, despite their capabilities in inferring rich contact information. This work considers the use of TacTip optical tactile sensors, mounted on a Model-O robotic gripper, in informing force-feedback haptics provided by a low-cost, open source haptic exoskeleton, called Remote Feelings. The exoskeleton design has been modified to further its capabilities in finger pose tracking and make the design less complex and more accessible. Deep learning and alternative methods are explored to estimate the contact forces on the tactile sensors which, combined with the forces sensed by the exoskeleton, is used to provide force feedback in a bilateral teleoperaion scenario.



## AUTHOR'S DECLARATION

I declare that the work in this dissertation was carried out in accordance with the requirements of the University's Regulations and Code of Practice for Research Degree Programmes and that it has not been submitted for any other academic award. Except where indicated by specific reference in the text, the work is the candidate's own work. Work done in collaboration with, or with the assistance of, others, is indicated as such. Any views expressed in the dissertation are those of the author.

SIGNED: ..... DATE: .....



20/04/2023



## TABLE OF CONTENTS

	Page
<b>List of Tables</b>	<b>vii</b>
<b>List of Figures</b>	<b>ix</b>
<b>1 Introduction</b>	<b>1</b>
1.1 Literature Review . . . . .	2
1.1.1 The Human Hand . . . . .	2
1.1.2 Haptic Feedback . . . . .	3
1.1.3 Tactile Sensing . . . . .	5
1.1.4 Tactile Model-O . . . . .	6
<b>2 Hardware</b>	<b>9</b>
2.1 Remote Feelings Haptic Exoskeleton . . . . .	9
2.1.1 Original Design and Limitations . . . . .	9
2.1.2 Hardware Modifications . . . . .	11
<b>3 Software</b>	<b>12</b>
3.1 Contact Force Estimation . . . . .	12
3.1.1 Tactile Image Processing . . . . .	12
3.1.2 Data Collection . . . . .	15
3.1.3 Deep Learning . . . . .	16
3.2 RF Kinematics and Control . . . . .	18
3.2.1 Finger Pose Estimation . . . . .	18
3.2.2 Force Feedback . . . . .	20
3.2.3 Teleoperation Framework . . . . .	23
<b>4 Results</b>	<b>25</b>
4.1 Contact Force Estimation Results . . . . .	25
4.1.1 Deep Learning Results . . . . .	25
4.1.2 Structural Similarity . . . . .	26
4.2 Remote Feelings and Teleoperation System Results . . . . .	27

---

**TABLE OF CONTENTS**

---

4.2.1	Free Motion Experiment . . . . .	27
4.2.2	Step Response Experiment . . . . .	28
4.2.3	Stiffness Rendering Performance . . . . .	29
4.2.4	Cost . . . . .	30
<b>5</b>	<b>Project Evaluation and Conclusion</b>	<b>31</b>
5.1	Discussion . . . . .	31
5.1.1	Remote Feelings Evaluation . . . . .	31
5.1.2	The Tactile Model-O and Teleoperation Framework Evaluation . . . . .	33
5.1.3	Force Estimation from Tactile Images Evaluation . . . . .	33
5.2	Future Work . . . . .	34
5.3	Conclusion . . . . .	35
<b>Bibliography</b>		<b>37</b>
<b>Appendix A</b>		<b>41</b>
Bill of Materials . . . . .		41

## LIST OF TABLES

TABLE	Page
3.1 Table containing the optimal blob detection parameters found by the cross-entropy optimisation procedure. . . . .	14
3.2 Table showing summary of force data collected. Also includes the SSIM calculations between the tactile images captured during the data collection and a reference image captured at the beginning of the data collection process. . . . .	16
4.1 Table showing the results from the deep learning. The values displayed are the MAE achieved on the relevant test set of tactile images in Newtons. Results are included for networks trained with images from just one sensors as well as a combined dataset of images from all three sensors. Furthermore, results are shown for the three image processing methods outlined in section 3.1.1. . . . .	25
4.2 MAE for force estimation using linear regression on SSIM between undeformed and deformed tactile images in Newtons. The regressions are displayed in figure 4.2. . . . .	27
1 Table containing the bill of material for the construction of the modified Remote Feelings haptic exoskeleton described in this work. . . . .	41



## LIST OF FIGURES

<b>FIGURE</b>	<b>Page</b>
1.1 Diagram showing the skeletal structure of the human hand, along with the relevant joints. Figure from [4]. . . . .	3
1.2 A selection of haptic feedback devices. From left to right, Mantis [3], CyberGrasp [32], DextrES [7] and the Senseglove DK1 [1] . . . . .	3
1.3 A selection of state-of-the-art optical tactile sensors and TacTip equipped Openhand grippers. From left to right, DiGiT [12], Gelsight Mini [37], the TacTip [13] and the TacTip-equipped M2 and GR2 grippers [36]. . . . .	5
1.4 A top down view of the T-MO showing the different fingers and the range of adduction/abduction in fingers 2 and 3 (Left) and an exploded view of the TacTips fitted to the distal phalanges of the T-MO (Right). Figures adapted from [9]. . . . .	7
2.1 a) The original RF design [8]. b) Modified, one-finger prototype. c) Completed, three-fingered RF redesign. . . . .	9
2.2 Circuit diagram for the electronics for the modified version of Remote Feelings alongside the resulting PCB design. . . . .	11
3.1 TacTip tactile images with various image processing effects applied. a) An unprocessed, grayscale image. b) A tactile image with a Gaussian adaptive threshold applied. c) The unprocessed image with the detected blobs overlaid. d) An image that uses the blob locations and sizes to exclude any parts of the image that are not the internal pins. . . . .	13
3.2 The hardware configuration used for the tactile image data collection, including a TacTip mounted to the distal phalange of the T-MO gripper being pressed against a Robotiq FT300 force/torque sensor mounted to the end-effector of a Dobot MG400 robot arm. . . . .	15
3.3 Flowchart outlining the data collection process for each finger on the T-MO. . . . .	16
3.4 Training and validation loss curves from training the CNNs using different image processing techniques and using datasets comprised of images from all sensors (combined) and individual sensors. . . . .	17

LIST OF FIGURES

---

3.5 Simplified diagram of the Remote Feelings exoskeleton and the human finger in 2 dimensions. $\theta_1$ , $\theta_2$ and $\theta_3$ denote the MCP, PIP and DIP joint angles of the finger respectively. $\zeta_1$ , $\zeta_1$ and $\zeta_3$ denote the fixed angles in the arm of the exoskeleton. $\phi_1$ , $\phi_2$ and $\phi_3$ denote the varying angles in the exoskeleton. $l_1$ to $l_3$ and $r_1$ to $r_6$ denote the link lengths forming the finger and the exoskeleton respectively. $s_Q$ denotes the position of the point on the distal phalange of the finger that the exoskeleton is attached to . . . . .	18
3.6 Simplified diagram of the RF exoskeleton for one finger, showing the forces acting upon the system at the fingertip and measured by the FSR. $O$ is the origin and corresponds to the point about which the servo motor pivots. The angles $\psi$ relate to the combinations of the fixed and variable exoskeleton joint angles as described in section 3.2.1. The curved, coloured arrows show the torques acting on each link in the exoskeleton's structure. Finally, $s_Q$ denotes the point at which the exoskeleton is attached to the user's finger. . . . .	20
3.7 Plot showing the collected data for the FSR calibration as well as the model that was fitted to the data. . . . .	21
3.8 Block diagrams showing the implementation of blocking and variable force feedback as described in section 3.2.2. . . . .	22
3.9 Diagram showing the teleoperation framework allowing RF to control the T-MO. Here, $I_T$ denotes the tactile images and $\hat{I}_T$ denotes the processed images. $F_T$ and $F_f$ denote the TacTip and fingertip forces respectively with $F_R$ being the difference between them and $F_{FSR}$ being the raw output from the FSR. The functions $f$ and $g$ denote the image processing and force transfer functions described in sections 3.1.1 and 3.2.2. Function $h$ denotes the force prediction from the processed tactile image. $\underline{\phi}$ denotes the joint angles of the exoskeleton and $\underline{\theta}$ the joint angles of the finger. $s_Q$ denotes the fingertip position and $\hat{\phi}_1$ is the angle for the servo motor to maintain to provide the FF. FK and IK respectively denote the forwards and inverse kinematics described in section 3.2.1 . . . . .	23
4.1 Scatter plots showing predicted force values against the ground truth on the relevant test set. The closer to the black line, the more accurate the prediction. Shown are three plots showing the performance of the CNNs trained on the combined dataset as well as three plots showing the predictions of the highest performing CNN trained on datasets formed of images from just one sensor. . . . .	26
4.2 Plots showing contact force against tactile image SSIM for all sensor and image processing combinations. Also shown as the black lines are linear models fitted to the displayed data. The accuracy of these models can be seen in table 4.2. . . . .	27

---

## LIST OF FIGURES

4.3 Results from the free motion experiment for each of the index and middle fingers as well as the thumb. The forces shown are measured by the FSRs during 4 cycles of curling and uncurling the fingers. . . . .	28
4.4 Results from the step response experiment for each of the index and middle fingers as well as the thumb. The forces shown are fingertip forces as well as the artificial contact force, simulating a sudden change in the estimated contact force on the TacTip. . . . .	29
4.5 T-MO grasping hard water bottle (a) and a soft, plush strawberry (b). . . . .	29
4.6 Histogram showing the calculated deviations applied to the servo angles, after the initial contact, for all fingers whilst performing a grasp of the two objects shown in figure 4.5, where the soft item is the strawberry and the firm item is the water bottle. . . . .	30



## INTRODUCTION

Tactile sensing is essential in the creation of robots with human-like dexterity [13]. Tactile sensors can be used to emulate a sense of touch, estimating contact forces, orientations, textures and more. Truly dexterous robots would be applicable in numerous scenarios where confident manipulation is required, e.g. in surgery or manipulation of delicate objects.

Haptic feedback can be broken down into cutaneous and force-feedback haptics. Cutaneous haptics emulates the sensation of touching an object by stimulating the user's RA, SA1 and SA2 mechanoreceptors in the skin. This feedback can provide information on the contact location, orientation and texture and how they change in time [24]. Force-feedback (FF), the focus of this project, is the reproduction of the sensation of pushing or squeezing an object. This allows a user to experience the size, shape and stiffness of a virtual or remote object. Applications include teleoperation, imitation learning, rehabilitation and virtual reality (VR) [34].

This project considers the confluence of tactile sensing and haptics. Specifically, this project aims to integrate a tactile Model-O (T-MO) [9] robotic hand with a low-cost haptic feedback exoskeleton, called Remote Feelings (RF) [8]. With a low cost of around \$300, the RF haptic exoskeleton is ideal for the exploration of low-cost haptics. The T-MO is equipped with TacTip optical tactile sensors in its distal phalanges. The use of deep learning (DL) is explored to infer the contact force on the TacTips from the tactile images. DL has been used previously in the estimation of the contact pose [14]. The estimated contact force is used to inform the FF algorithm governing the haptic exoskeleton. The aim is to provide accurate FF to the user to enable gentle, remote grasping and stiffness perception for applications in teleoperation.

A three-fingered, modified version of the RF haptic exoskeleton has been constructed, including changes to the electronics and the addition of rotary encoders on all the joints to enable precise tracking of the user's fingers using forwards and inverse kinematics. Furthermore, a

force analysis of the system has been carried out to ascertain the force applied to the exoskeleton by the user, at the fingertip, whilst not directly measuring it. The T-MO, along with a Dobot MG400 robot arm and a Robotiq FT-300 force/torque sensor has been used to collect a large number of tactile images, from the TacTips, in order to train a DL model to estimate the contact force on each finger from the corresponding tactile images. To this end, various image processing techniques and models have been trialled in order to provide the best trade-off between inference speed and accuracy. Once the data were collected, the resulting models can be combined with the RF control algorithm, along with the finger pose calculation to control the T-MO and feed the forces estimated by the gripper back to the user. Finally, a number of experiments are carried out to assess the performance of the system, including the quality of free motion whilst utilising RF, the exoskeleton's response to a sudden change in contact force, the allowed deviation of the users' fingers whilst grasping objects of varying stiffness and a qualitative assessment of the quality of the stiffness rendering.

This project is distinct from existing work due to the integration of the three main hardware components. TacTips have seen little use in the field of teleoperation and have yet to be integrated with a haptic feedback device. Furthermore, the low cost and accessibility is emphasised since this is a key limitation in the widespread adoption of haptic devices [3]. All of the hardware is constructed with 3D printed and off-the-shelf components, with the designs being open source.

The remainder of this thesis provides a review of the relevant literature, a summary of the main hardware components followed by an explanation of the software controlling and linking the hardware together. Finally, a thorough performance evaluation is carried out, followed by an exploration of possible future work, a discussion of the key findings and a conclusion.

## 1.1 Literature Review

### 1.1.1 The Human Hand

The morphology and features of a haptic feedback glove must be closely related to the structure of the human hand, the system it is designed to interact with. The human hand (including the wrist) is often modelled with 23 degrees of freedom (DoF) where each DoF corresponds to a basic motion of a joint. Systems, like the human hand, are capable of complex motion through actuating a combination of DoFs.

Figure 1.1 shows the skeletal structure of the hand, including the joints. Each finger, except the thumb, is comprised of three bones, the distal, proximal and intermediate phalanges. These phalanges are joined by three joints, the meta-carpophalangeal (MCP), the proximal-interphalangeal (PIP) and the distal-interphalangeal (DIP). Each MCP joint is capable of extension/flexion and adduction/abduction, giving it two DoFs, whereas the PIP and DIP joints are only capable of extension/flexion and therefore one DoF. The thumb has only one inter-phalangeal (IP) joint, an MCP joint as well as the trapezio-metacarpal (TM) joint. The thumb's IP and MCP joint

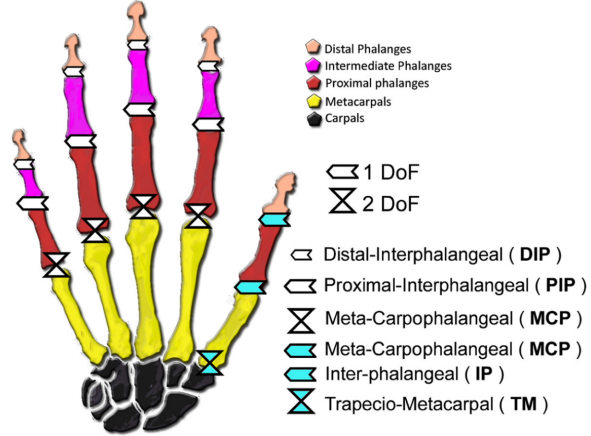


Figure 1.1: Diagram showing the skeletal structure of the human hand, along with the relevant joints. Figure from [4].

are capable of extension/flexion and the TM joint both extension/flexion and adduction/abduction [4]. Therefore, each finger, including the thumb has a total of four DoFs. The additional three DoFs in the wrist are not considered in this work.

### 1.1.2 Haptic Feedback

Force-feedback haptic devices can be categorised as grounded and ungrounded. Grounded devices are attached to a rigid object such as a wall. These devices, including Mantis [3] (seen in figure 1.2) and PHANToM [20], will often have more DoFs and can produce higher fidelity haptic sensations due to their use of larger, heavier and more precise actuators. A limitation of the grounded approach is the restricted workspace. Feedback can only be provided within the range of the mechanical linkage used. Ungrounded devices aim to combat this by anchoring the device to another point on the user. This is seen in wearable exoskeletons and gloves. Such devices include CyberGrasp, Dexmo [34] (both presented in figure 1.2) and the RML glove [19].



Figure 1.2: A selection of haptic feedback devices. From left to right, Mantis [3], CyberGrasp [32], DextrES [7] and the Senseglove DK1 [1]

Often found in human-robot interaction (HRI) systems, compliance control is commonly applied in the field of haptics. Amongst FF gloves and exoskeletons, the two main types of compliance control, impedance and admittance control, can be seen. CyberGrasp [32] and the

Senseglove DK1 [1] use impedance control [28] where the position of the fingers is the input and the actuators output a force. CyberGrasp achieves this with an external actuator assembly that transfers the FF through bowden tubes, whereas, the Senseglove DK1 utilises strings and magnetic friction brakes [4]. In contrast, admittance control [28] takes force as an input and outputs a position for the actuator. Examples include the RML glove [19], which uses force sensors at the fingertips, Remote Feelings [8], which uses force sensing resistors (FSRs) embedded in the servo housing and the BMIFOCUS HES [31] which uses a load cell and a modified admittance control algorithm that utilises intent detection. An advantage of admittance control devices is that they only require position controlled actuators, which are typically of lower weight and cost.

A third form of FF exists in braking or blocking devices. These devices do not render varying stiffness but create a binary distinction between free motion and completely blocked motion. Such devices include the LucidGlove [33] and Dexmo [6] which use servo motors to engage the brakes. Due to a reliance on mechanical friction to oppose motion, rather than the actuator itself, lower powered and cheaper actuators can be used. However, this is at the expense of fidelity and contact stiffness feedback.

Literature exists on the application of haptic feedback technologies in teleoperation. The torque feedback from servo motors in a robot arm is utilised in [27] to inform feedback provided by a PHANToM haptic device. The FF was found to be less accurate as the load on the arm increased due to limitations in the motors' torques. Similarly, authors in [25] use the motor torques in a three-fingered BarrettHand to inform FF provided by a CyberGlove. The kinematic differences in the robotic and human hand were accounted for using force and position mappings. Once again, the quality of the FF was found to be limited by the maximum torque measurable by the BarrettHand. Authors in [11] assess the impact, on performance, in a teleoperation task of moving boxes and blocks, of varying degrees of feedback including no feedback, blocking FF and substituted vibrotactile feedback. The feedback was informed using Optoforce 3D force sensors. No difference was found in performance between feedback and no feedback, although the majority of the participants preferred some kind of feedback. Furthermore, the blocking FF was found to be frustrating by some participants due to them being unable to tighten their grip once a contact force was detected, leading to unstable grasps.

Linked to teleoperation, the effects of FF haptics on providing demonstrations for imitation learning has been explored in the literature. Imitation learning is a method for policy optimisation which utilises demonstrations from a domain expert, usually a human, to inform the learning. This method is often used in manipulation tasks when an optimal solution cannot be manually defined. In contact-rich tasks, providing FF to the demonstrator allows the collection of more informative and accurate demonstrations, especially if the robot is to be force controlled. The use of a combination of kinesthetic demonstration (manually guiding the robot arm) and further demonstrations using a FF haptic device is explored in [10]. The kinesthetic demonstrations are used to inform the position control of a robot arm and the haptic demonstrations are used

to inform the force control, allowing the robot to carry out complex tasks including ironing and opening a door. Authors in [5] use grounded, FF haptics to provide demonstrations for learning. The haptic device is utilised to improve the quality of the demonstrations and act as a method of bi-directional communication between the robot and the demonstrator. It is noted that this approach is particularly useful when the robot is located remotely and other methods of demonstration, such as kinesthetic, are unavailable.

### 1.1.3 Tactile Sensing

Several different technologies have been developed to tackle the problem of tactile sensing in robotics, such as piezoelectric, magnetic and optical sensors. An example of a tactile sensor using piezoelectrics is developed in [17]. This skin-like sensor is capable of distinguishing multiple different stimuli such as slipping, bending and touching. It can do this while maintaining a rapid response time (10ms), less than that of human skin. Tactile sensors using magnets include those developed in [30] and [21]. The former describes uSkin, a soft, force-sensing (up to 6N) skin that can cover large areas. Magnets embedded in a soft material move when a force is applied and this is detected using a series of Hall Effect sensors. The latter uses magnetoresistive sensors embedded in a soft, elastomer fingertip that, alongside a single magnet, can measure contact forces up to 5N.

The use of soft, elastomer fingertips is commonly adopted amongst optical tactile sensors. These sensors aim to extract tactile information from images of the deformation of the soft surface, resulting in high sensitivity, spatial resolution and lower cost [12]. Optical tactile sensors include DiGiT and GelSight (shown in figure 1.3). These sensors have been used for manipulating a marble in an Allegro robotic hand, measuring a human's pulse and more [12, 37].



Figure 1.3: A selection of state-of-the-art optical tactile sensors and TacTip equipped Openhand grippers. From left to right, DiGiT [12], Gelsight Mini [37], the TacTip [13] and the TacTip-equipped M2 and GR2 grippers [36].

Tactile sensing has seen use in informing cutaneous haptics. Authors in [29] use two participants, one equipped with tactile sensors and the other with an electro-tactile stimulation glove. They explored the application of remote training, with tactile sensations being transferred between the trainer and the trainee. Tactile sensing and haptics has also seen extensive use in

surgery. Tactile sensing is used, in [16] to control soft actuators placed at a surgeon’s fingertips to enable the remote identification of tumour tissue. Similarly, authors in [23] use a combination of haptic technologies and a BioTac tactile sensor to detect the orientation of a stick embedded in emulated heart tissue. The feedback was found to significantly improve the participants’ performance.

The TacTip is an optical, biomimetic, tactile sensor that uses physical internal pins, mimicking the dermal papillae in human skin, that are deformed upon the application of a force. These sensors are constructed using multi-material 3D printing with their designs being open-source. The customisability of the design has resulted in variations of the sensor being applied in numerous scenarios including goal-driven pushing, slip detection, tactile servoing and even as feet for mobile robots [13]. Interpretation of the images produced by these sensors is often done using DL [14] since every pixel contains information on the deformation of the soft surface.

Several robotic grippers have been equipped with various TacTips to extend their grasping capabilities. These include the fully actuated Shadow Modular Grasper and the anthropomorphic, underactuated Pisa/IIT SoftHand [13]. The Shadow Modular Grasper uses the TacTips to estimate contact orientations to obtain stable grasps and the Pisa/IIT SoftHand to ensure a light grip on an unknown, held object as well as estimating the poses of edge features on held objects.

TacTips have also been integrated with various robotic grippers from the Yale Grablab [18]. These grippers are in keeping with the 3D-printed, low-cost and open-source philosophy of the TacTip. The Openhand M2 and GR2 grippers were equipped with custom TacTips (shown in figure 1.3) in order to carry out object reorientation and rolling [36]. Furthermore, the highly adaptable morphology of the TacTip can be seen in the creation of the large Tac-Thumb for the M2 gripper [35]. Most relevant to this project, TacTips have been attached to an Openhand Model-O robotic gripper [9], creating the Tactile Model-O (T-MO).

#### 1.1.4 Tactile Model-O

A 3D-printed, open-source version of the iHY hand [22], the Openhand Model-O, with its three fingers and 4 DoFs has been shown to be capable of power grasps, fingertip grasps and basic in-hand manipulation by utilising the underactuated nature of its construction. Underactuation allows the gripper to deform around held objects while using few actuators, simplifying the hardware, software as well as reducing the cost. The original Model-O can be configured with either a pivot and a flexure joint in each finger or two pivot joints. These joints are actuated by braided polythene wires, wound around pulleys mounted on MX-28T Dynamixel servo motors. A fourth and final motor controls the adduction/abduction of the fingers opposing the thumb, which move together through a mechanical linkage, constituting the fourth DoF.

In the creation of the T-MO, the double pivot finger design was chosen and a number of modifications were made. Most importantly, the distal phalanges are replaced with custom TacTips. Each sensor contains 30 internal pins, 3D-printed using multi-material printing. This

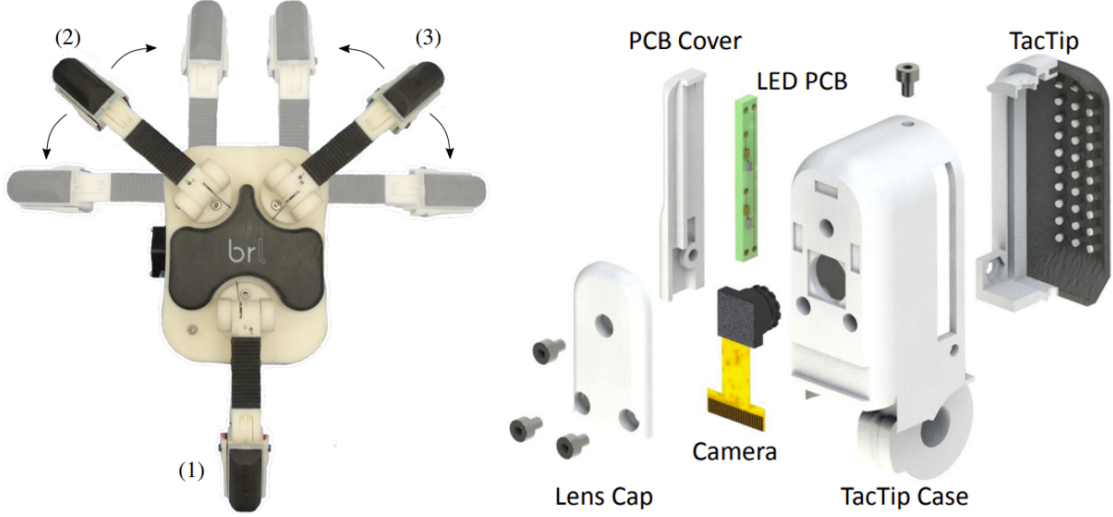


Figure 1.4: A top down view of the T-MO showing the different fingers and the range of adduction/abduction in fingers 2 and 3 (Left) and an exploded view of the TacTips fitted to the distal phalanges of the T-MO (Right). Figures adapted from [9].

technique allows multiple materials to be printed and combined together to create highly precise morphologies. The soft fingertips are printed in Tango Black and the housings, as well as the pin-tips, are printed in Vero White plastic. The contrast in colours allows for more robust inference from the tactile images. Once printed, the sensors are filled with RTV27905 silicone contained behind an acrylic lens. The TacTips were designed to be as close as possible in shape to the original distal phalanges to maintain the strong grasping performance. However, increasing the width from 12mm to 35mm to include the TacTips was unavoidable. This results in reducing the ability to pick up thin and flat objects, such as coins, which the original Model-O was capable of.

The compact nature of these sensors requires an appropriately compact and performant camera system. For this, Jevois A33 machine vision cameras were selected along with anti-distortion lenses with a field of view of 90°. These camera systems allow the bulk of the electronics to be housed in the main body of the T-MO, with only the camera sensor and a small breakout PCB needing to be mounted to the distal phalange, connected with a ribbon cable. Another advantage of these camera systems is their ability to carry out on board computation using OpenCV and other common machine learning libraries, such as TensorFlow Lite. This means that the majority of the tactile image processing can be offloaded to the cameras themselves, increasing performance through parallelisation and by reducing the load on the host computer. In [9], it was found that offloading item classification to each camera system and then taking the mean of the predictions resulted in a 2% drop in classification accuracy, compared to the use of a high performance host PC, but this would allow the T-MO to operate autonomously and untethered.

The authors in [9] outlined a number of potential improvements to the design, including reducing the thickness of the distal phalanges in order to restore the ability to pick up thin, flat objects. This could be done through utilising mirrors, allowing the camera to be placed closer to the sensing surface of the TacTip, as seen in the GelSlim sensor [2]. Furthermore, it is noted in [9] that these custom TacTips have notably fewer pins than other sensors in the family and this may limit their performance. Other potential improvements to the TacTips could include thinner skin or a non-uniform pin distribution, although it is stated that the optimal morphology is likely to be task dependent. Implementing such changes is outside the scope of this project but could form the basis of future work.

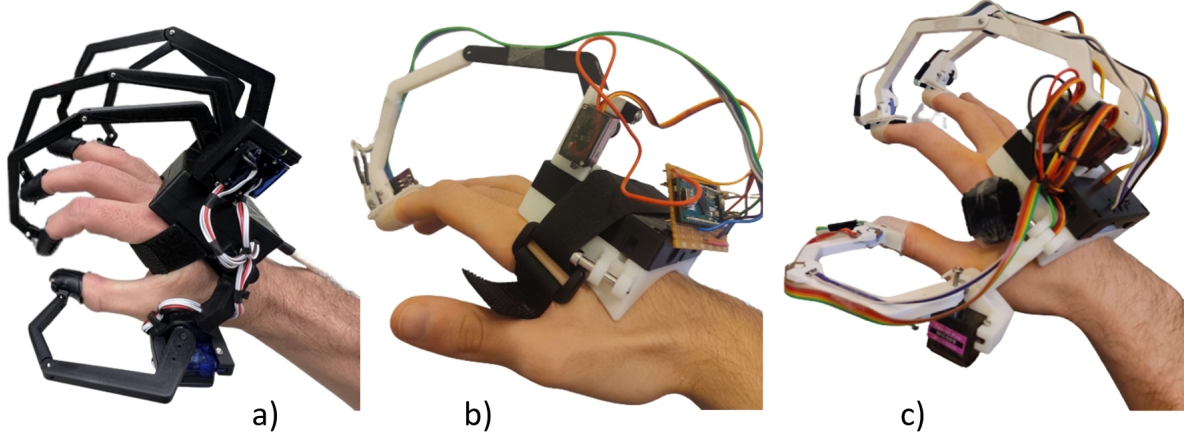
**HARDWARE****2.1 Remote Feelings Haptic Exoskeleton**

Figure 2.1: a) The original RF design [8]. b) Modified, one-finger prototype. c) Completed, three-fingered RF redesign.

**2.1.1 Original Design and Limitations**

The original design of the RF haptic exoskeleton (shown in figure 2.1a) is comprised of a series of mechanical linkages between the fingertips of the user and the servo motors, mounted on the dorsal side of the hand, making it an example of ungrounded haptics. The actuators used are low-cost, hobby servo motors (such as the TowerPro MG90s) which have a stall torque of 1.8kg-cm (0.1765Nm). This is adequate to provide force feedback to the fingers. These servos have been

modified such that the internal encoder can be read directly by the microcontroller (an ESP32) so that the true position of the motor shaft can be used in the software. This is achieved using custom PCBs, replacing the ones originally in the servo motors.

As outlined in 1.1, in order to provide variable stiffness feedback, it is necessary to include force-sensing capabilities in the design of the haptic device. These cheap servo motors are unable to provide torque-feedback to the controller, therefore another sensor is required. The original RF design utilises force-sensitive resistors (FSRs). When a force is applied, a flexible semiconductor substrate is pressed against another substrate covered in current-carrying dots, lowering the resistance. When assembled in a voltage-divider with a pull-down resistor (10K) they can be used on an analogue input pin of the selected microcontroller. The main advantages are the small size, low electrical complexity and low cost. However, FSRs are not precise force measuring devices and their readings may not be fully time independent in the presence of a constant force, due to the soft nature of their construction. Indeed, they are commonly used to measure the presence or absence of a force, rather than quantifying it. In the original RF design, the FSRs are mounted between the servo motors and their 3D-printed housing. The motors are mounted on a pivot and are pressed against the FSR by a spring. As the user attempts to move their finger, the spring is compressed and the FSR's resistance increases as the force applied to it decreases. This deviation in FSR reading is used in a proportional controller to adjust the position of the corresponding servo and therefore the user's finger.

The design has advantages in its accessibility and low cost of around \$300, although the authors note that this would be greatly reduced if the electronic components were purchased in bulk [8]. Regardless, this is significantly more affordable than other offerings such as the SenseGlove Dk1 (\$3000) and CyberGrasp (\$5000) [4]. The authors outline a number of limitations in the design [8]. Firstly, the UART communication protocol that was selected introduced numerous errors in the ESP32 microcontroller, resulting in a delay needing to be added in software to ensure the messages are fully sent and received. This work mitigates this by replacing the microcontroller and utilising simple serial communication to the host PC, where the bulk of the processing will occur. A further issue identified was the non-linearity in the force application to the fingertip with respect to the finger pose. As the finger curls more, the servo motor applies a lower force to the user. They identified the use of torque-controllable motors as a potential solution, however, this would increase the cost, complexity and weight. Finally, the use of a non-invertible op-amp circuit was identified as a potential solution to the non-linear response of the FSRs' resistance with respect to the force applied. This would also work to increase the electronic complexity and cost of the system and, therefore, simpler calibration methods will be explored.

## 2.1. REMOTE FEELINGS HAPTIC EXOSKELETON

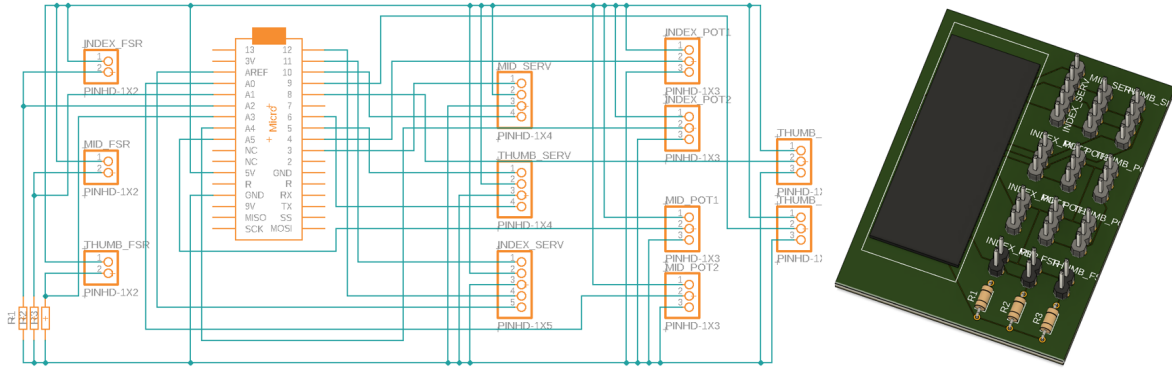


Figure 2.2: Circuit diagram for the electronics for the modified version of Remote Feelings alongside the resulting PCB design.

### 2.1.2 Hardware Modifications

In recreating the RF haptic device for this project, a number of modifications have been made. Firstly, the number of fingers that the feedback is provided to has been reduced to three, the index and middle fingers and the thumb. This is simply due to the fact that the T-MO has only three fingers itself. The thumb corresponds to finger 1 on the T-MO and the index and middle fingers corresponds to fingers 3 and 2 respectively, as seen in figure 1.4. This reduction resulted in requiring fewer input pins on the selected microcontroller and therefore an Arduino micro has been chosen due to the simplicity in programming it and the ease of purchase.

Similarly to the original design, the servo motors have been modified to provide their true position. Rather than using a custom PCB, wires can be directly soldered to the encoder pins within the servo motors. These internal encoders use a reference voltage of 2.41V, which is stepped down from the 5V which is used to power the motors. Therefore, one of the motors requires an additional wire that provides this reduced voltage to the external reference voltage pin on the Arduino. Therefore, the other motors require only one additional wire, carrying the position signal from the internal encoders. This can be seen in the circuit diagram in figure 2.2. In order to measure the other angles in the exoskeleton arms, Murata SV01 encoders were used due to their small size, low friction and low cost.

It can be seen from the one-fingered prototype (figure 2.1) that the manufacture of a simple, double-sided PCB was necessary to counteract the number of wires. The design was generated using Fusion 360, from the circuit diagram, and both can be seen in figure 2.2.

In order to tackle the issue of the non-linear force with respect to the finger position, a thorough kinematic and force analysis of the system has been carried out. By using the encoders to find the pose of the exoskeleton and assuming (whilst the user is experiencing feedback) that the system is static, the force exerted by the user on the end of the exoskeleton can be calculated. Details and calculations are presented in section 3.2.2.

## SOFTWARE

This project uses various pieces of software to tie the hardware components together. These include the use of machine learning techniques to infer contact forces from tactile images, various image processing techniques, forwards and inverse kinematics for finger pose estimation and a framework for teleoperation using RF and the T-MO.

### 3.1 Contact Force Estimation

In order to use tactile sensing inform FF haptics, it is first necessary to obtain force measurements from the sensors. TacTips have no specialised force-sensing capabilities, however, their tactile images contain rich contact information including texture, sensor pose and shear forces.

In the literature, inferring contact information from the tactile images is often done using deep learning [14]. Therefore, many tactile images must be obtained, through a data collection procedure, and processed into a form appropriate for insertion into a neural network which can then be trained to estimate the contact force. Alternative force estimation methods are also explored, including the use of structural similarity (SSIM) in the images.

#### 3.1.1 Tactile Image Processing

In order to obtain high-quality measurements from tactile images, it is necessary to process the images. A variety of techniques have been applied in the literature and, here, four main options are explored in order to find the best approach when considering accuracy, robustness and computational feasibility.

All image processing methods begin with the capture of a grayscale frame from each TacTip at a resolution of 320 by 240. Since the tactile information in the images is present largely in

the internal pin positions, these images are then cropped to a resolution of 90 by 240 so that the frame only contains the TacTip’s pins. The use of a higher resolution may improve the deep learning performance, however, for this comparably low number of pins the gains are minimal. The literature outlines further image processing methods to isolate the pins in the frame.

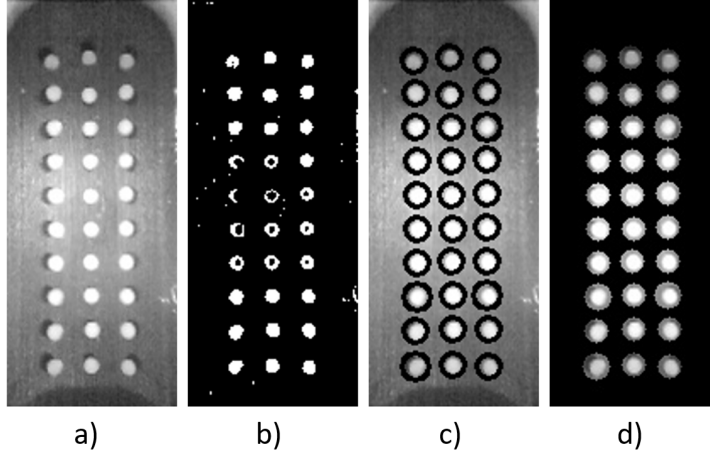


Figure 3.1: TacTip tactile images with various image processing effects applied. a) An unprocessed, grayscale image. b) A tactile image with a Gaussian adaptive threshold applied. c) The unprocessed image with the detected blobs overlaid. d) An image that uses the blob locations and sizes to exclude any parts of the image that are not the internal pins.

The first approach is to apply a thresholding method to the tactile images. Thresholding takes either individual pixel values, or the sum of pixel values over a region, and compares this to a threshold. If the threshold value is greater than the value obtained from the pixel, that pixel will be set to 0. Thresholding methods that use the same threshold for each pixel are called global thresholding methods. However, if the lighting conditions across the image are not constant, the result may be undesirable. To combat this, adaptive thresholding can be used, which is when a threshold value is calculated for a given local region.

Gaussian adaptive thresholding is an adaptive thresholding method where the threshold value,  $T$ , is calculated for each pixel as,

$$(3.1) \quad T = \text{mean}(I_L) - C,$$

where  $I_L$  denotes a local region about the pixel in question,  $C$  is a constant that can be used for fine-tuning and  $\text{mean}()$  denotes the Gaussian mean function. The size of the region  $I_L$  can also be modified for best results. Using the arithmetic mean would result in each pixel in the region being weighted the same, whereas, the Gaussian mean results in pixels located further away from the centre of  $I_L$  contributing less to the calculation of  $T$ . This method has been used in [26], also to process tactile images before their input into a CNN. The parameters chosen to apply the thresholding to the T-MO’s TacTip’s images are  $C = -25$  and the radius of the region  $I_L$  is set at 15. An example of this method, applied to a tactile image, can be seen in figure 3.1.

Another approach is the use of a blob detection algorithm. A blob refers to a region of pixels, in an image, that are connected by some property, such as pixel intensity. The blob detection algorithm is comprised of four main steps. Firstly, the input image is thresholded using a range of threshold values, resulting in multiple binary images. Then, in each thresholded image, white pixels that are adjacent to one another are grouped. The centres of these blobs in the binary images are computed and the binary images are merged such that blobs in different images that have centres closer than some threshold value are combined. Finally, the centres and radii of the blobs in the merged image are calculated.

It is possible to filter the types of blobs that are detected through the use of the parameters; circularity, convexity and inertia ratio. Circularity is calculated as  $4\pi A/p^2$  where  $A$  is the area of the proposed blob and  $p$  is its perimeter. Convexity is defined as the ratio between the area of the proposed blob and the area of its convex hull. Finally, inertia ratio is the ratio between the minor and major axes of the proposed blob. Higher inertia ratio means the blob is more circular.

In order to obtain the optimal blob detection parameters, a cross-entropy optimisation method is used. The objective function, to be minimised, is simply  $L(\underline{p}) = 30 - B$ , where  $\underline{p}$  is a vector of the detection parameters and  $B$  is the number of blobs detected. The optimal blob detection parameter for each sensor can be seen in table 3.1.

TacTip	Index	Middle	Thumb
Min Threshold	20.3	48.1	25.8
Max Threshold	176.3	235.4	161.2
Min Area	23.2	42.0	33.4
Max Area	131.2	109.8	156.9
Min Circularity	0.495	0.475	0.453
Min Inertia	0.453	0.537	0.553
Min Convexity	0.71	0.658	0.382

Table 3.1: Table containing the optimal blob detection parameters found by the cross-entropy optimisation procedure.

Once the blobs have been detected, either the raw blob positions can be used as an input into a regression model, or an image mask can be constructed to isolate the pin positions in the original tactile images. An example of a tactile image with detected blobs overlaid the unprocessed greyscale image as well as an image masked using the blob locations and sizes can be seen in figure 3.1.

Structural similarity index measure (SSIM) is a simple and robust method for quantifying the difference between two tactile images. It has been used in [26] and [9] for quantifying the sensor deformation and for contact detection respectively. It is calculated as,

$$(3.2) \quad \text{SSIM}(u, v) = \frac{(2\mu_v\mu_u + c_1)(2\sigma_{uv} + c_2)}{(\mu_u^2 + \mu_v^2 + c_1)(\sigma_u^2 + \sigma_v^2 + c_2)},$$

where  $u$  and  $v$  represent regions in the compared images of size  $N \times N$  (here  $N = 7$ ).  $\mu$  and  $\sigma$

represent the mean and variance of the pixel values in  $u$  or  $v$  respectively, with  $\sigma_{uv}$  denoting the covariance between both regions. Finally,  $c_1$  and  $c_2$  denote regularisation constants which take the values  $(0.01L)^2$  and  $(0.03L)^2$  where  $L = 255$  which is the dynamic range of the pixel values in the images. The regions  $u$  and  $v$  are slid across the images and the resulting similarity scores are averaged to provide a final value of SSIM. To facilitate SSIM comparisons whilst the T-MO is in use, upon initialisation, a reference, undeformed image is captured and saved to provide a reference point for further comparisons.

Each of the aforementioned image processing techniques are used in the creation of a training set for a CNN. Performance metrics for each of the methods can be seen in section 4.1.1. The highest performing image processing technique is selected for use in the teleoperation framework proposed in section 3.2.3.

### 3.1.2 Data Collection

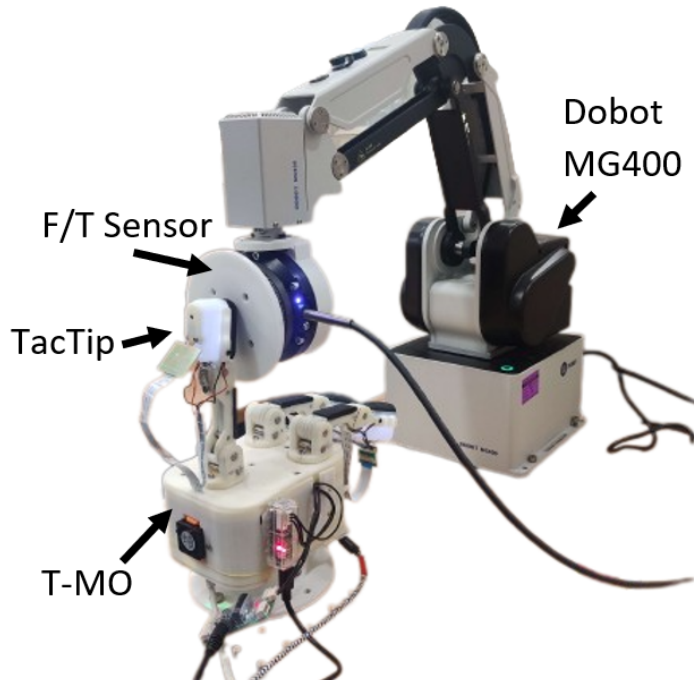


Figure 3.2: The hardware configuration used for the tactile image data collection, including a TacTip mounted to the distal phalange of the T-MO gripper being pressed against a Robotiq FT300 force/torque sensor mounted to the end-effector of a Dobot MG400 robot arm.

Each TacTip will have slightly different physical properties, lighting conditions and wear. Therefore, it is necessary to collect a dataset of tactile images from each sensor.

Index		Middle		Thumb	
	SSIM		SSIM		SSIM
<b>Min</b>	0.617	0.071	0.673	0.267	0.734
<b>Max</b>	0.842	4.21	0.833	1.91	0.852
<b>Mean</b>	0.722	1.36	0.749	0.802	0.803
<b>Std</b>	0.037	0.500	0.019	0.221	0.024
					0.533

Table 3.2: Table showing summary of force data collected. Also includes the SSIM calculations between the tactile images captured during the data collection and a reference image captured at the beginning of the data collection process.

The data collection process uses a FT-300 F/T sensor, mounted to the end-effector of a Dobot MG400 robot arm. This arm, as well as the T-MO, is mounted to a rigid board. A picture of this apparatus can be seen in figure 3.2. The F/T sensor is moved to a position, upon which the chosen T-MO finger will capture a reference image and begin to close. First contact between the fingertip and the F/T sensor is registered when the SSIM between the reference image and the most recently captured tactile image dips below some threshold.

This position of first contact is saved as the minimum finger position. The maximum is set at a fixed value greater than this. The TacTip on the T-MO fingertip is repeatedly tapped against the F/T sensor, with increasing levels of force until the finger closure reaches the previously specified maximum value. Finally, the F/T sensor is moved to a new position and the process is carried out again. This process is outlined in figure 3.3.

Moving the F/T sensor to different positions and rotations aims to facilitate the capture of contact forces at varying levels of finger flexion and whilst deforming different regions of the TacTip. This should make the resulting model more robust when objects of different sizes and shapes are being grasped. Data collection will use 10 force levels for 30 F/T sensor positions, each with 10 different rotations resulting in 3000 data for each TacTip.

A summary of the data collected for each TacTip can be seen in table 3.2. This includes both the force data and the SSIM values calculated from the tactile images captured during the data collection.

### 3.1.3 Deep Learning

Previous work, [14] has shown the potential of CNNs in obtaining data from tactile images. The architecture outlined describes a series

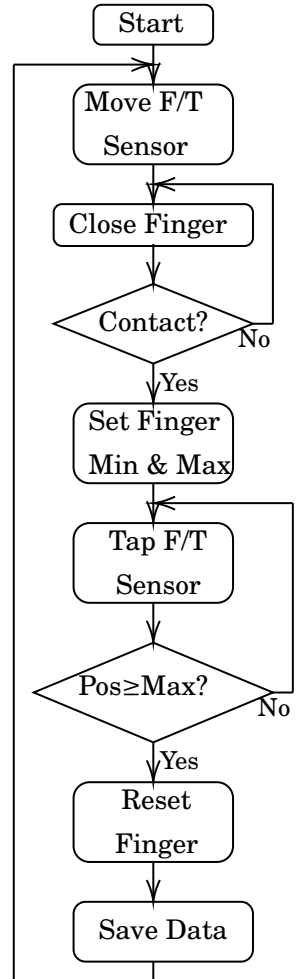


Figure 3.3: Flowchart outlining the data collection process for each finger on the T-MO.

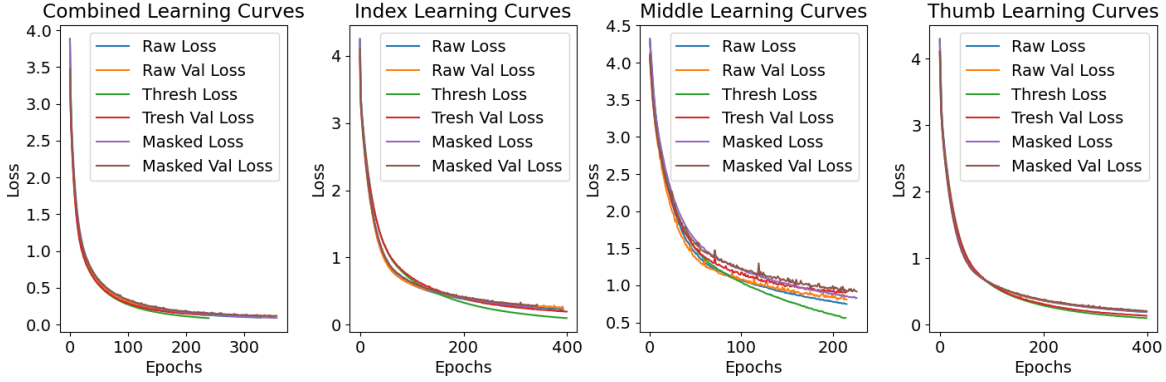


Figure 3.4: Training and validation loss curves from training the CNNs using different image processing techniques and using datasets comprised of images from all sensors (combined) and individual sensors.

of convolutional layers followed by a series of fully connected layers. This has shown strong performance in regressing relative poses of tactile sensors using tactile images. Typically one network is trained per sensor [14, 26] due to their differing characteristics, however, due to the similarities in the three TacTips on the T-MO, training a network with a combined dataset of images from all three sensors is also explored. During teleoperation this will allow the force estimation to utilise less of the GPU memory of the host PC and predictions can be generated simultaneously by querying the network with a batch comprised of one image from each sensor.

The contact force is estimated by a CNN comprised of 4 convolutional layers (each with 256 filters) followed by a fully connected layer with a width of 128. As in [14], mean-squared error (MSE) is used as the loss function and the Adam optimiser is selected. The force labels are scaled by removing the mean and scaling the data to have unit variance before training. A network is trained, for each TacTip and a combination of all three, on each of the unprocessed, cropped images, the thresholded images and the images obtained through the blob detection and masking process.

Each network is trained over a maximum of 400 epochs, using 90% of the 3000 tactile images for training and 5% for both the test and validation sets. In order to prevent overfitting, l1 and l2 regularisation methods are employed (with coefficients of 0.0001 and 0.01 respectively) as well as batch normalisation after each convolutional layer. Furthermore, the validation set is used for early stopping of the training to prevent overfitting.

The learning curves for each of the networks described can be seen in figure 3.4. It can be seen that, for all combinations of image processing and dataset composition, learning occurs as the loss drops significantly over the epochs. A complete evaluation of the performance of all the trained networks can be seen in section 4.1.1.

## 3.2 RF Kinematics and Control

Two main methods of control and feedback are investigated using the RF haptic glove. Firstly, the basic blocking FF method is implemented, followed by extending this to provide variable levels of FF. In both cases, in order to provide accurate FF and finger pose estimation, thorough kinematic and force analyses are required.

### 3.2.1 Finger Pose Estimation

As outlined in section 2.1.2, the addition of encoders to the exoskeleton allows the pose of the finger to be calculated. Firstly, the fingertip position can be obtained using forward kinematics (FK) along the exoskeleton and then the finger pose is obtained using inverse kinematics (IK) from the fingertip position to the MCP joint of the finger or thumb.

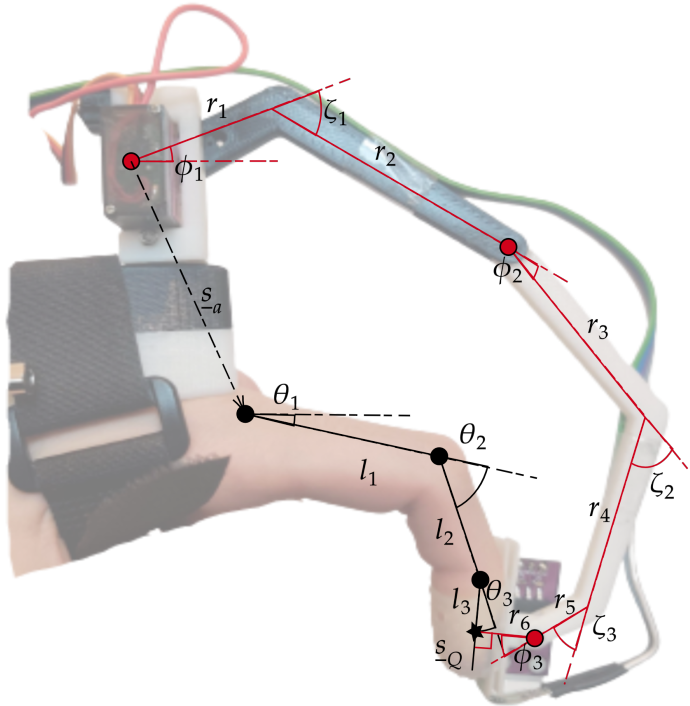


Figure 3.5: Simplified diagram of the Remote Feelings exoskeleton and the human finger in 2 dimensions.  $\theta_1$ ,  $\theta_2$  and  $\theta_3$  denote the MCP, PIP and DIP joint angles of the finger respectively.  $\zeta_1$ ,  $\zeta_2$  and  $\zeta_3$  denote the fixed angles in the arm of the exoskeleton.  $\phi_1$ ,  $\phi_2$  and  $\phi_3$  denote the varying angles in the exoskeleton.  $l_1$  to  $l_3$  and  $r_1$  to  $r_6$  denote the link lengths forming the finger and the exoskeleton respectively.  $s_Q$  denotes the position of the point on the distal phalange of the finger that the exoskeleton is attached to.

From Figure 3.5, it can be seen that the position of the finger-RF connection,  $s_Q$ , is related to both the finger joint angles,  $\underline{\theta} = [\theta_1, \theta_2, \theta_3]^T$  and the exoskeleton joint angles, which are comprised of the rotational joints,  $\underline{\phi} = [\phi_1, \phi_2, \phi_3]^T$ , and mechanically fixed joints,  $\underline{\zeta} = [\zeta_1, \zeta_2, \zeta_3]^T$ . The joint

denoted  $\phi_1$  is the actuated joint for each finger whilst  $\phi_2$  and  $\phi_3$  are passive joints. The joints denoted  $\theta_1$ ,  $\theta_2$  and  $\theta_3$  correspond to the MCP, PIP and DIP joints of the human finger respectively.

Without loss of generality, the FK can be simplified by combining the exoskeleton joint angles,  $\underline{\phi}$  and the fixed exoskeleton angles  $\underline{\zeta}$  as the vector  $\underline{\psi}$  such that  $\psi_1 = \phi_1 + \zeta_1$ ,  $\psi_2 = \phi_2 + \zeta_2 + \zeta_3$  and  $\psi_3 = \phi_3$ . Similarly, the joint lengths are combined such that  $a_1$  is the distance between  $\phi_1$  and  $\phi_2$ ,  $a_2$  is the distance between  $\phi_2$  and  $\phi_3$  and  $a_3 = r_6$ . Therefore, the fingertip position relative to the MCP joint of the finger,  $\underline{s}_Q$ , is calculated as,

$$(3.3) \quad \underline{s}_Q = \begin{bmatrix} a_1 \cos(\psi_1) + a_2 \cos(\psi_1 + \psi_2) + a_3 \cos(\psi_1 + \psi_2 + \psi_3) \\ a_1 \sin(\psi_1) + a_2 \sin(\psi_1 + \psi_2) + a_3 \sin(\psi_1 + \psi_2 + \psi_3) \end{bmatrix} + \underline{s}_a.$$

The structure of the thumb exoskeleton differs slightly, however, the position of the thumb's tip can be obtained through the same calculation by setting  $a_3 = \psi_3 = 0$ .

Upon obtaining the position of the fingertip, IK can be used to provide the pose of the human finger through the joint angles,  $\underline{\theta}$ . Firstly, the sum of the finger angles is known due to the maintained right angle connection between the finger and the exoskeleton. This results in  $\theta_1 + \theta_2 + \theta_3 = \psi_1 + \psi_2 + \psi_3 - \frac{\pi}{2}$ .

Then, the position of the DIP joint, relative to the MCP joint, is

$$(3.4) \quad \begin{bmatrix} x_{DIP} \\ y_{DIP} \end{bmatrix} = \underline{s}_Q - \frac{1}{2} \begin{bmatrix} l_3 \cos(\theta_1 + \theta_2 + \theta_3) \\ l_3 \sin(\theta_1 + \theta_2 + \theta_3) \end{bmatrix}.$$

Therefore, the angle between the horizontal and the straight line between the MCP and DIP joints,  $\alpha = \arctan(y_{DIP}/x_{DIP})$ .

Consider the triangle formed by the three finger joints. Letting  $\beta = \pi - \theta_2$  and using the cosine rule, the distance of the DIP joint from the MCP joint,  $r$  (where  $r^2 = x_{DIP}^2 + y_{DIP}^2$ ), can be determined as

$$(3.5) \quad r^2 = l_1^2 + l_2^2 - 2l_1l_2 \cos(\beta).$$

Therefore the angle at the PIP joint,  $\theta_2$ , can be determined as

$$(3.6) \quad \theta_2 = \pi - \beta = \pi - \arccos\left(\frac{l_1^2 + l_2^2 - x_{DIP}^2 - y_{DIP}^2}{2l_1l_2}\right).$$

Similarly, considering the same triangle, let angle  $\gamma = \alpha - \theta_1$ . Therefore,

$$(3.7) \quad r^2 = l_1^2 - 2rl_1 \cos(\gamma) = l_2^2,$$

which can be used in the calculation of  $\theta_1$  as,

$$(3.8) \quad \theta_1 = \alpha - \gamma = \arctan\left(\frac{y_{DIP}}{x_{DIP}}\right) - \arccos\left(\frac{x_{DIP}^2 + y_{DIP}^2 + l_1^2 - l_2^2}{2l_1\sqrt{x_{DIP}^2 + y_{DIP}^2}}\right).$$

Since the sum of the finger angles is known,  $\theta_3$  can be determined using the values for  $\theta_1$  and  $\theta_2$ .

The above derivations are true for both the middle and index fingers. The process for the thumb varies slightly as it only has a single IP joint. Therefore, the inverse kinematics differs in there being only two angles required to obtain the thumb pose.

### 3.2.2 Force Feedback

In order to provide accurate force feedback, it is necessary to calculate the force experienced by the system from the user, at the fingertip. This will also work to combat the limitation in the RF design outlined in 2.1.

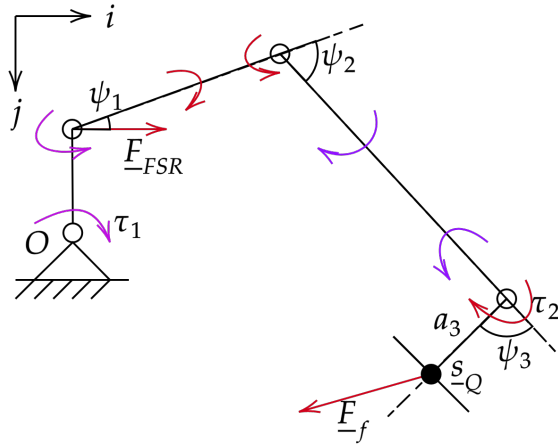


Figure 3.6: Simplified diagram of the RF exoskeleton for one finger, showing the forces acting upon the system at the fingertip and measured by the FSR.  $O$  is the origin and corresponds to the point about which the servo motor pivots. The angles  $\psi$  relate to the combinations of the fixed and variable exoskeleton joint angles as described in section 3.2.1. The curved, coloured arrows show the torques acting on each link in the exoskeleton's structure. Finally,  $s_Q$  denotes the point at which the exoskeleton is attached to the user's finger.

To calculate the fingertip force,  $F_f$ , we must first assume that, whilst RF is providing feedback, the system is static. Therefore, the fingertip force, must be such that it counteracts the translational forces and torques on the system. The translational forces acting on the system are the force measured by the FSR,  $F_{FSR}$ , and gravity. Gravity is disregarded due to the fact that the exoskeleton linkages are lightweight and any effects of gravity are unlikely to change the overall user experience. Therefore, it can be seen from figure 3.6 that the fingertip force must have an equal and opposite component in the  $i$  direction to the force measured by the FSR, simply  $[-|F_{FSR}|, 0]^T$ .

The servo motors used in the design do not provide torque feedback to the microcontroller. However, it is possible to use the FSR reading,  $F_{FSR}$ , to estimate the torque that the motor is both experiencing and outputting. Considering the link in figure 3.6 that connects the point  $O$  to

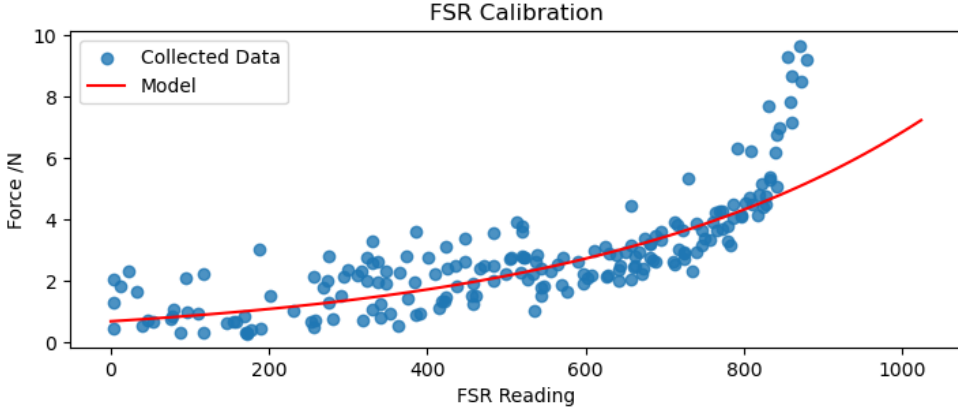


Figure 3.7: Plot showing the collected data for the FSR calibration as well as the model that was fitted to the data.

the  $\psi_1$  joint and noting that  $\underline{F}_{FSR}$  acts perpendicularly to this link, it is possible to calculate the torque  $\tau_1$  as  $\tau_1 = 0.02|\underline{F}_{FSR}|$  where 0.02 is the length of this link in metres.

Since the system is considered to be static and each joint is assumed to be frictionless, this torque propagates down the exoskeleton structure and, therefore, the fingertip force must apply the opposite torque along the exoskeleton. The component of  $\underline{F}_f$  that provides this torque acts perpendicularly to the final link in the exoskeleton, connecting  $s_Q$  and the  $\psi_3$  joint, and has a magnitude of  $\tau_1/a_3$  where  $a_3$  is the length of the final exoskeleton link. This component of  $\underline{F}_f$  acts in the direction defined as  $[-\sin(\alpha), -\cos(\alpha)]^T$  where  $\alpha = \pi - \psi_1 - \psi_2 - \psi_3$ .

Therefore, by combining the translational and rotational forces, it is possible to obtain the fingertip force as,

$$(3.9) \quad \underline{F}_f = \begin{bmatrix} -|\underline{F}_{FSR}| \\ 0 \end{bmatrix} - \frac{\tau_1}{a_1|[-\sin(\alpha), -\cos(\alpha)]^T|} \begin{bmatrix} \cos(\alpha) \\ \sin(\alpha) \end{bmatrix}.$$

The final component in this force calculation is obtaining a force, in Newtons ( $|\underline{F}_{FSR}|$ ), from the FSR reading  $R_{FSR}$ . The FSR is connected to an analogue input pin of the microcontroller and reports values in the range [0, 1024]. The FSR was placed atop the F/T sensor and a range of force values is obtained by manually compressing the FSR and therefore the F/T sensor. The range of F/T values and FSR readings can be seen in figure 3.7 and the most appropriate model of the relationship was found to be,

$$(3.10) \quad |\underline{F}_{FSR}| = 0.6867e^{0.0023R_{FSR}},$$

using the maximum likelihood estimate method to find the constants.

Visually, from figure 3.7 it can be seen that the model does not fit the data well for larger force values. This is unlikely to be problematic during deployment due to the fact that forces that large are likely to overpower the servo motors' maximum torque.

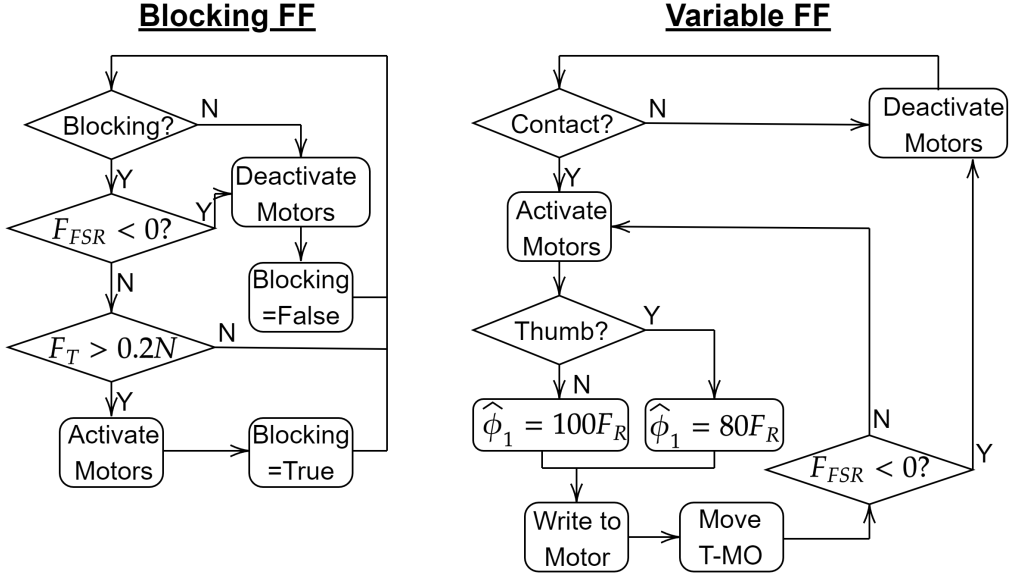


Figure 3.8: Block diagrams showing the implementation of blocking and variable force feedback as described in section 3.2.2.

To provide blocking FF, the system simply needs to block the user's finger movements when a significant enough contact is detected by the T-MO's TacTips. This is simply done by deactivating the servo motors when the user's movement is supposed to be unobstructed and activating them and fixing their position when feedback is to be provided. However, to provide more realistic teleoperation functionality, the blocking must be automatically disengaged when the system detects the user removing their grasp. This detection can be done by waiting until a negative FSR force is detected and then disengaging the servo motors.

To provide variable force feedback, the exoskeleton must allow some movement of the user's fingers after the initial contact to simulate the compression of the grasped object. Initially, the variable feedback works the same as the blocking feedback, engaging the servo motors when a contact is detected and disengaging when a negative FSR force is measured. However, after the initial contact, the difference between the force estimated at the TacTip,  $F_T$ , and the fingertip force,  $F_f$ , is calculated to obtain  $F_R$ , or the resultant force. This value is multiplied in a simple P controller by the values 100 and 80 for the middle/index fingers and the thumb respectively to obtain the servo deviation,  $\hat{\phi}_1$ , in microseconds, for the servos' PWM signals. These constants were tuned experimentally whilst carrying out grasps of different objects, to allow for a clear distinction between sensations of grasping the objects. The thumb requires a lower proportional constant since it is shorter and thus requires a lower deviation to simulate the compression of the grasped object. The value of  $\hat{\phi}_1$  is added to the position maintained by the servo for the corresponding finger, allowing further movement of the user's fingers after the initial contact. Both methods of feedback are independently applied to each finger such that grasps using any subset of the three fingers is possible.

### 3.2.3 Teleoperation Framework

Before active teleoperation can begin, the RF haptic exoskeleton must undergo a calibration procedure for the FSR and to relate the finger pose to a signal for controlling the T-MO. Since the FSRs are clamped between the servo motors and their 3D printed housings, when no external force is acting upon the exoskeleton, the FSRs will return a non-zero force. To find this force, during initialisation, the user is instructed to hold their fingers still, then 20 FSR readings are taken and the average of these values is subtracted from subsequent readings to determine the external forces.

Each finger of the T-MO is controlled by a one-dimensional signal in the interval  $[0, 1]$  (where 0 corresponds to a fully open finger and 1 corresponds to a fully closed finger). To obtain such a signal from the pose of the operator's fingers further calibration is required. Upon initialisation, the user is prompted to fully open their fingers. The forwards and inverse kinematics are carried out to determine the pose of the finger. This is repeated for the finger in its fully closed position. The sum of the finger angles ( $\theta$ ) in each configuration is stored. During operation, this minimum and maximum value is used to scale subsequent sums of finger angles into the closed interval  $[0, 1]$  which is used to control the position of the corresponding finger on the T-MO.

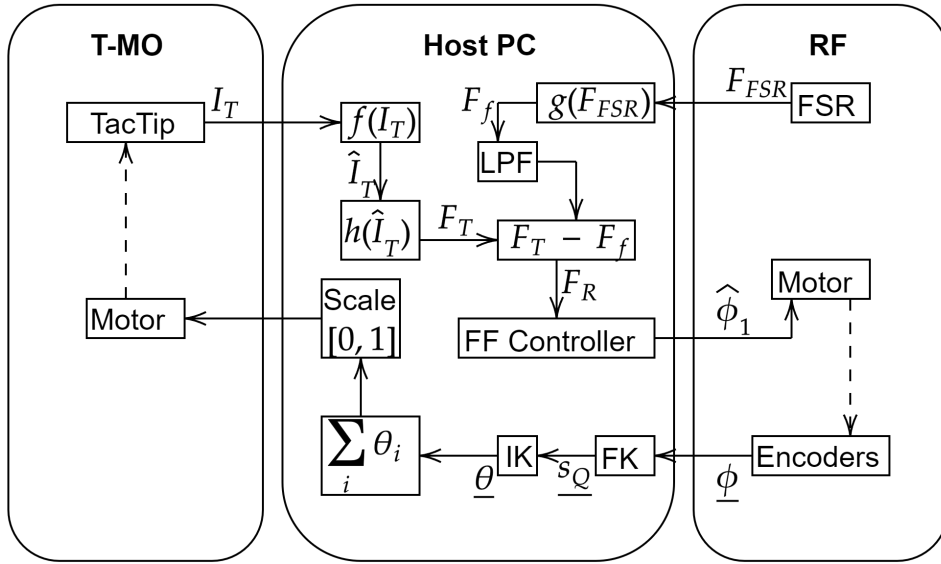


Figure 3.9: Diagram showing the teleoperation framework allowing RF to control the T-MO. Here,  $I_T$  denotes the tactile images and  $\hat{I}_T$  denotes the processed images.  $F_T$  and  $F_f$  denote the TacTip and fingertip forces respectively with  $F_R$  being the difference between them and  $F_{FSR}$  being the raw output from the FSR. The functions  $f$  and  $g$  denote the image processing and force transfer functions described in sections 3.1.1 and 3.2.2. Function  $h$  denotes the force prediction from the processed tactile image.  $\underline{\phi}$  denotes the joint angles of the exoskeleton and  $\underline{\theta}$  the joint angles of the finger.  $s_Q$  denotes the fingertip position and  $\hat{\phi}_1$  is the angle for the servo motor to maintain to provide the FF. FK and IK respectively denote the forwards and inverse kinematics described in section 3.2.1

After calibration, the teleoperation can proceed as outlined in figure 3.9. The software is designed to be multithreaded, with a thread for reading images for each TacTip, a thread to estimate the contact forces, a thread for monitoring the serial connection to RF and a thread for the overarching control of the system, henceforth referred to as the main thread. Each TacTip captures images at 40 FPS, processes them, and stores them in memory accessible by the force estimation thread which can then generate predictions.

Meanwhile, the thread monitoring the serial communication with RF, is constantly receiving the FSR and pose data from the microcontroller and replying with the desired feedback,  $\hat{\phi}_1$ . When blocking FF is implemented, this is a binary value for each finger instructing the microcontroller to either engage or disengage the relevant motor. If variable FF is used, this value will be a angular deviation from the initial contact point for the servo motor to enact in order to allow movement of the user's fingertip.

At each time step, in the main thread, the most up to date pose, FSR and contact force estimation data is read from the other threads. The exoskeleton pose data is used to calculate the finger pose and subsequently the signal controlling the position of the corresponding T-MO finger. The FSR data (which is passed through a low-pass filter to counteract the high-frequency noise in these sensors) and contact force estimation are used in the FF controller to determine the appropriate action for RF. This information is sent to the serial communication thread which will be sent to RF in the next serial message.

# C H A P T E R



## RESULTS

### 4.1 Contact Force Estimation Results

#### 4.1.1 Deep Learning Results

The evaluation errors obtained from each network can be seen in table 4.1. Scatter plots showing the individual predictions on the test set can be seen in figure 4.1. This includes plots showing performance of each of the three image processing techniques when used in a network trained with combined images as well as the highest performing networks and image processing techniques used to train the individual sensor networks.

It can be seen that the highest performance with a combined training set is with no image processing with an MAE of 0.1012N. For the individual sensor networks, the highest performance is obtained from no processing for the index sensor (0.1214N), masking with blobs for the middle

<b>Training Set:</b>	Combined				Index	Middle	Thumb	
	<b>Sensor:</b>	Index	Middle	Thumb	Average	Index	Middle	Thumb
<b>Image Type:</b>	<b>Raw</b>	0.1139	0.1069	0.08292	0.1012	0.1214	0.1040	0.08990
	<b>Thresholded</b>	0.1390	0.1104	0.1021	0.1171	0.1310	0.1049	0.08912
	<b>Masked with Blobs</b>	0.1172	0.1137	0.08869	0.1107	0.1320	0.1019	0.08484

Table 4.1: Table showing the results from the deep learning. The values displayed are the MAE achieved on the relevant test set of tactile images in Newtons. Results are included for networks trained with images from just one sensors as well as a combined dataset of images from all three sensors. Furthermore, results are shown for the three image processing methods outlined in section 3.1.1.

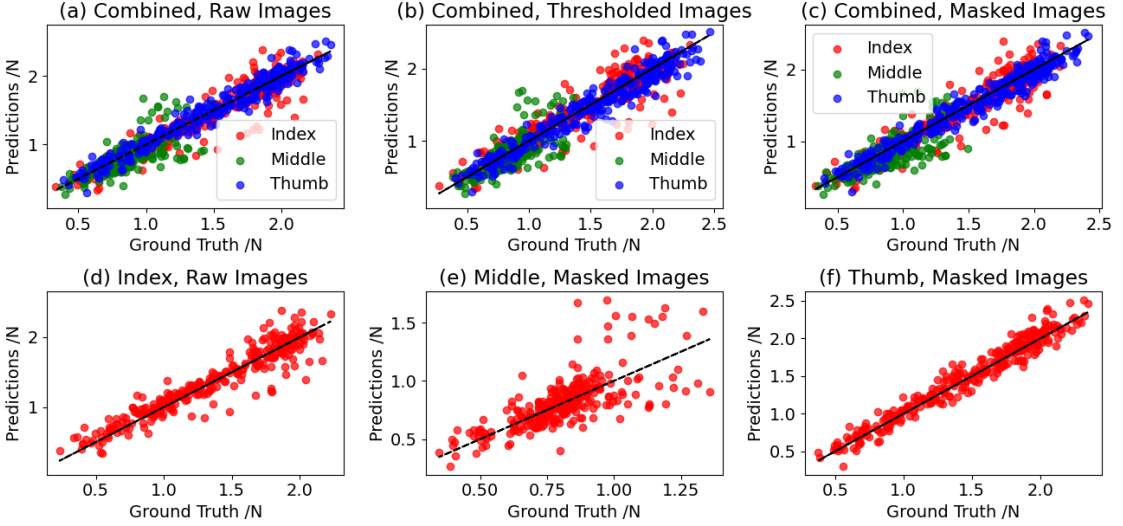


Figure 4.1: Scatter plots showing predicted force values against the ground truth on the relevant test set. The closer to the black line, the more accurate the prediction. Shown are three plots showing the performance of the CNNs trained on the combined dataset as well as three plots showing the predictions of the highest performing CNN trained on datasets formed of images from just one sensor.

sensor (0.1019N) and the thumb sensor (0.08484N). The best performing CNN trained with the combined dataset outperforms the highest performing individual sensor dataset CNNs for the index and middle sensors. This suggests that increasing the size of the training set has a greater impact on improving performance than the differences in the sensors does to decrease it, for these two sensors, suggesting the CNN is able to generalise across images from different sensors. This pattern is not observed with the thumb sensor which obtains its highest performance when only images from that sensor are used for training.

#### 4.1.2 Structural Similarity

Due to use in previous work in quantifying the deformation of the TacTip and detecting contacts [15, 26], it is hypothesised that there is a strong relationship between contact force and SSIM.

Figure 4.2 shows the relationship between contact force and SSIM for the images collected during the data collection. It also contains linear regressions fit to the data, with the MAE for these models shown in table 4.2.

It can be seen that the relationship between SSIM and contact force differs between the sensors, with the index and middle fingers showing a much more linear relationship than the thumb. This is reflected in the errors shown in table 4.2. Comparing tables 4.2 and 4.1 it can be seen that the DL approach generates predictions with a lower error across all sensor and dataset combinations considered.

## 4.2. REMOTE FEELINGS AND TELEOPERATION SYSTEM RESULTS

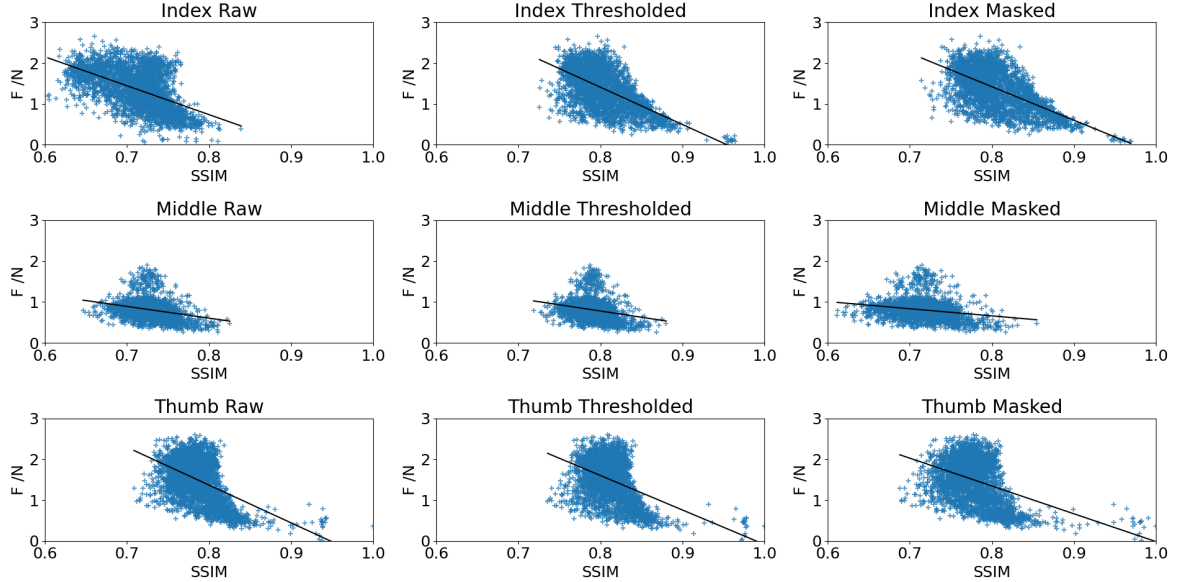


Figure 4.2: Plots showing contact force against tactile image SSIM for all sensor and image processing combinations. Also shown as the black lines are linear models fitted to the displayed data. The accuracy of these models can be seen in table 4.2.

Image Type	Index	Middle	Thumb
<b>Raw</b>	0.3397	0.1448	0.3979
<b>Thresholded</b>	0.3186	0.1452	0.4122
<b>Masked</b>	0.3176	0.1465	0.4186

Table 4.2: MAE for force estimation using linear regression on SSIM between undeformed and deformed tactile images in Newtons. The regressions are displayed in figure 4.2.

These results show the efficacy of estimating contact forces from TacTip tactile images using a variety of techniques. A full discussion of these results can be seen in section 5.1.

## 4.2 Remote Feelings and Teleoperation System Results

### 4.2.1 Free Motion Experiment

During typical operation, whilst no feedback is being provided to the user, the exoskeleton should provide minimal opposition to the motion of the user. This opposition to the user's motion comes from friction in the joints of the exoskeleton, gravity acting on the exoskeleton and the exoskeleton's inertia [19]. To quantify the quality of the free motion allowed by RF, a simple experiment can be carried out. The user is instructed to open and close their fingers in a controlled manner whilst force data from the FSRs are recorded and stored. Truly free, unopposed motion would see no force reading from the FSRs. Note, the force recorded here is the force measured

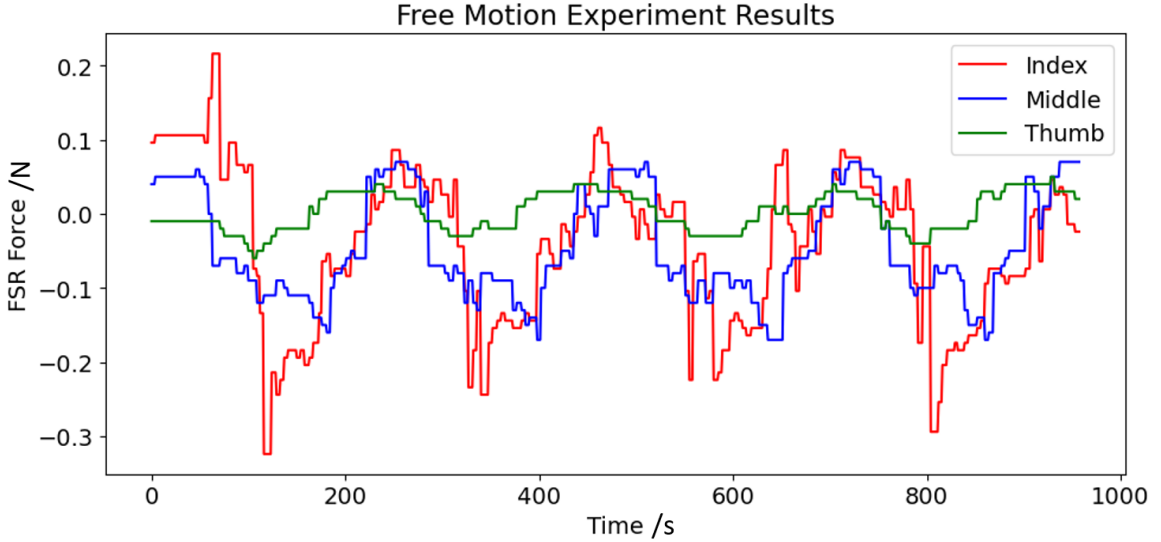


Figure 4.3: Results from the free motion experiment for each of the index and middle fingers as well as the thumb. The forces shown are measured by the FSRs during 4 cycles of curling and uncurling the fingers.

directly by the FSR, not the fingertip force, since the calculation of the fingertip force assumes the system is static.

Results from this experiment can be seen in figure 4.3. It can be seen that each of the three fingers is subject to friction during free motion. Both the index and middle fingers experience roughly equivalent opposition to motion during the closing of the fingers (the peaks in the lines displayed in figure 4.3). The index finger experiences more friction during the release of the grasp (shown in the troughs in figure 4.3) than the middle finger and the thumb.

#### 4.2.2 Step Response Experiment

In order to quantify the speed and accuracy with which the RF exoskeleton responds to a sudden change in the estimated contact force on the corresponding TacTip, a step response experiment can be carried out [19]. The user is instructed to slowly close their finger and, at a certain point, an artificial, constant contact force is input to the system. Ideal operation would see the fingertip force rising rapidly to the value of this artificial contact force. Once the fingertip force exceeds the artificial contact force, further increase in the fingertip force should be offset by the servo motor deviating, allowing further movement of the user's finger, whilst the fingertip force stays close to the artificially provided force.

Results for such an experiment for each finger can be seen in figure 4.4. The estimated fingertip force rises to meet the artificial contact force for each of the user's fingers. This is done most rapidly by the middle finger, meeting the contact force after approximately 0.25s. The

#### 4.2. REMOTE FEELINGS AND TELEOPERATION SYSTEM RESULTS

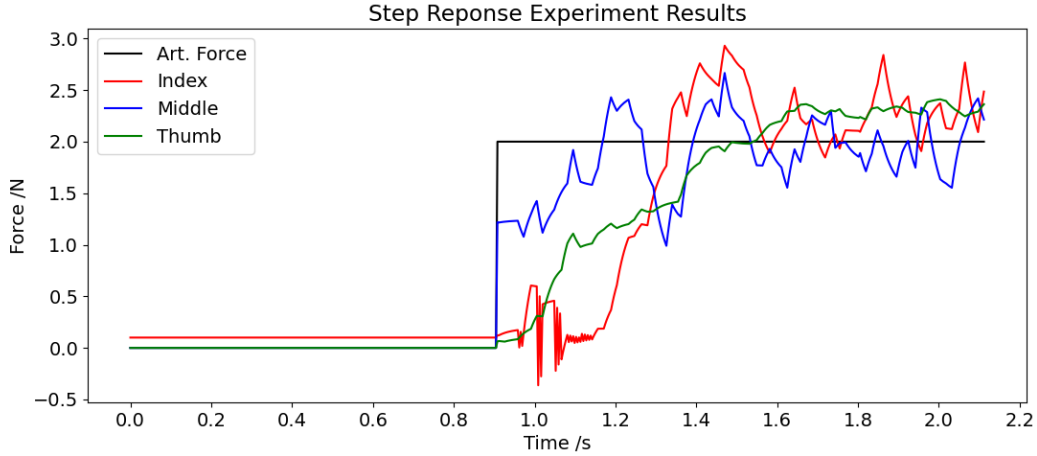


Figure 4.4: Results from the step response experiment for each of the index and middle fingers as well as the thumb. The forces shown are fingertip forces as well as the artificial contact force, simulating a sudden change in the estimated contact force on the TacTip.

thumb is the slowest, taking around 0.6s to meet the artificial force and the index finger takes around 0.4s. After reaching the artificial force, it can be seen that the force increase measured at each fingertip tapers off as the servos begin to deviate from the initial contact location. The middle fingertip force oscillates around the artificial force value of 2N whilst the index and thumb fingertip forces oscillate around 0.3N above this value.

#### 4.2.3 Stiffness Rendering Performance

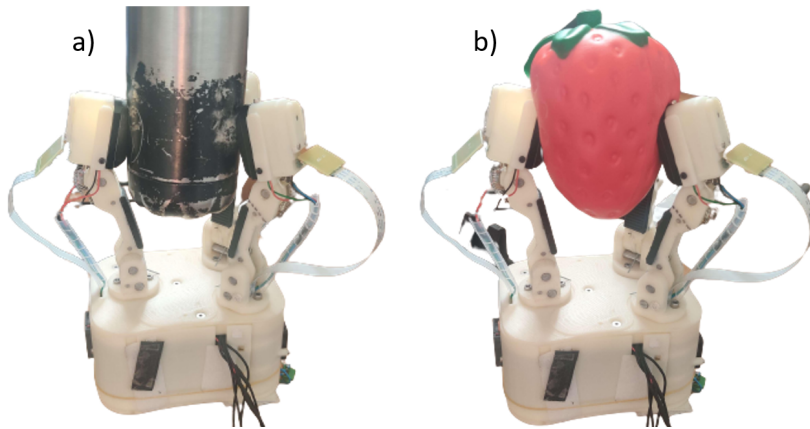


Figure 4.5: T-MO grasping hard water bottle (a) and a soft, plush strawberry (b).

In order to quantify the performance of RF in rendering objects with different stiffnesses being grasped by the T-MO, the servo deviations ( $\hat{\phi}_1$ ) can be recorded during grasps of objects with different stiffnesses. Since a less stiff object will deform more under the same contact force,

it is expected that grasping softer objects should allow for a greater deviation in the fingertip position and therefore the servo angle. For reasons outlined in section 5.1, the combination of image SSIM and a linear model is used for the contact force estimation in this experiment.

Figure 4.5 shows the objects selected for this experiment. Two objects with a differing stiffnesses are selected. Each object is grasped by controlling the T-MO with RF. After initial contact, any subsequent motion in the T-MO is due to the deviation ( $\hat{\phi}_1$ ) that is calculated from the measured forces. Using RF, the grasp is tightened until the motors in the T-MO reach their maximum torque upon which the grasp is released and the time series of servo deviations is saved. Figure 4.6 shows the distribution of values of  $\hat{\phi}_1$  recorded during the grasping of each object over 5 experiments.

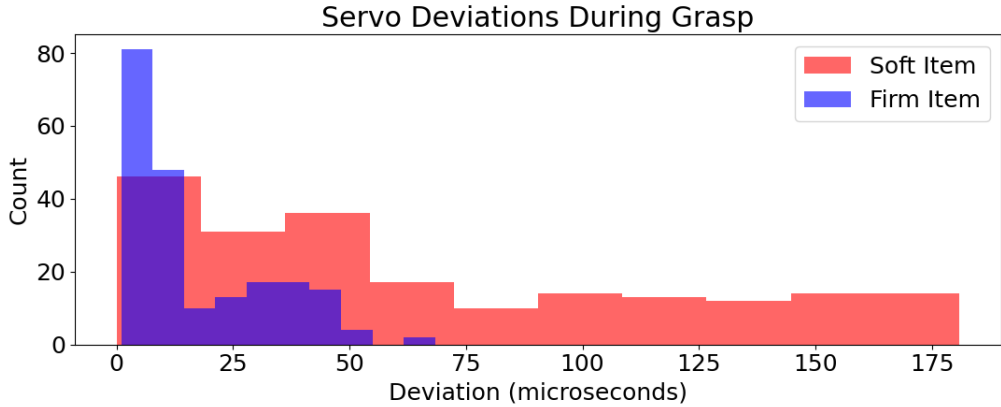


Figure 4.6: Histogram showing the calculated deviations applied to the servo angles, after the initial contact, for all fingers whilst performing a grasp of the two objects shown in figure 4.5, where the soft item is the strawberry and the firm item is the water bottle.

#### 4.2.4 Cost

The total cost of the modified RF haptic exoskeleton is £92.91 and the full break down can be seen in the bill of materials (BOM) shown in table 1 in appendix 6.

There remains room to further reduce the cost, most notably through purchasing some of the components in bulk, such as the torsion spring and the FSRs, however, the BOM displays low-quantity prices since this is more realistic should a recreation of this RF version be attempted.

CHAPTER



## PROJECT EVALUATION AND CONCLUSION

### 5.1 Discussion

#### 5.1.1 Remote Feelings Evaluation

The modifications to the RF hardware outlined in section 2.1 are successful in furthering the capabilities of the exoskeleton as well as reducing the cost. The addition of the joint encoders to the exoskeleton arms allows the calculation of the finger poses which can be used to obtain the configuration of the user's hand. This is applicable in teleoperation as well as in VR where accurate hand poses can form the basis of more fine control. This is also key for addressing the issue of non-linear fingertip force with respect to finger pose. The calculations for calculating the fingertip force from the FSR force (shown in section 3.2.2) utilise the pose data afforded by the addition of the encoders.

Another key modification is the move to the more accessible Arduino platform. This reduces the overall cost and the complexity of the electronics required. The electronics can be entirely assembled by hand with no need for surface mount components. However, should the design be extended back to 5 fingers, a new approach to the electronics such as the use of a multiplexing circuit will be required due to the limited number of analogue input pins on the Arduino Micro.

A key part of the original design that has remained is the use of FSRs for measuring the forces experienced by the exoskeleton. The limitations in these components remain including their lack of full time-independence and general imprecision that can be seen in figure 3.7. They do not directly provide a force measurement and therefore imprecise calibration is required through the use of a model fitted to data. The model shown in figure 3.7 has provided adequate performance for initial experimentation, but with a low  $R^2$  value of 0.68 it is clear that it does not provide the accuracy that would be required for tasks involving precise forces or for rehabilitation.

As outlined in section 4.2.4, despite modifications including the addition of further electronics, the overall cost of the modified RF has been reduced to a total of £92.91. Compared to existing commercial solutions such as the Senseglove DK1 and CyberGrasp, the cost of RF is found to be 30 and 50 times lower respectively [4]. Compared to the cost of the original RF design (\$300 [8]), this modified version is even lower. This is largely due to the reduction to three fingers as well as the simplification of the electronics used. A downside of the low-cost approach is the low durability, particularly of the servo motors. Overloading the motors with a strong grasping force may damage their internal gearboxes, requiring a replacement motor. This resulted in three broken motors over the course of this project. However, despite this, due to the low price and ease of purchase of the components, it is clear that the modified RF satisfies the criteria for being low-cost and accessible.

Authors in [19] identify 200mN as an acceptable level of force experienced by the user during free motion, however, this force is measured at the fingertip so a direct comparison cannot be drawn with the results obtained in figure 4.3. However, the forces shown in figure 4.3 rarely exceed this value and user feedback does not identify the opposition to motion as problematic during teleoperation. The thumb appears to experience the lowest friction during operation. This is likely due to some of the forces being absorbed by the spring used to keep the thumb servo housing in contact with the MCP joint of the thumb. The free motion performance could be improved through actively driving the servos to follow the user's fingers at all times, as done in the original design [8]. However, this could work to hinder the user's movements should they attempt to rapidly change the pose of a finger, faster than the exoskeleton can respond.

The step response results shown in figure 4.4 show that, in the presence of a rapid change in contact force, the fingertip forces measured by RF will quickly rise to meet it, before levelling off, showing the efficacy of the variable force feedback implementation. This also suggests that the fingertip force calculation outlined in section 3.2.2 works well to rectify the non-linearities in the FSR response with respect to the pose of the finger. However, compared to response of the RML glove [19] the response time is slow (0.3s compared to 0.03s). Furthermore, undesirable oscillations can be seen in the fingertip forces, shortly after the application of the artificial force, which may result in inconsistent FF and, in a worst case, vibrations detectable by the user when the servo attempts to adjust to the rapid changes in measured force. This is due to the low cost servos which sometimes noticeably vibrate when a load is applied. Furthermore, it can be seen that the thumb is less prone to experiencing high amplitude oscillations in the measured force due to the spring holding the servo against the MCP joint.

It can be seen that (from figure 4.6), whilst grasping the soft object, the servos deviate significantly more from the position of first contact, with the histogram showing a much wider distribution than for the firm object. This demonstrates that the teleoperation system is successfully able to distinguish between two objects with differing stiffnesses, and reporting this information to the user in the form of a larger deviation of the finger position from the first contact.

The results from the free motion, step response and teleoperation experiments show that the RF redesign shows promise as a low-cost alternative to existing FF devices, however, the performance reduction compared to offerings such as the RML glove disqualify this modified RF exoskeleton from tasks requiring a high degree of precision in the FF. Therefore, the RF haptic exoskeleton is best suited for use in VR and teleoperation where very precise FF is not required. The FF implementation is sufficient to distinguish between objects of different stiffnesses but is lacking if precise manipulation is required. Furthermore, this device is not suitable for use in rehabilitation due to the human fingers not being actively driven and the imprecision in the force measurements.

### 5.1.2 The Tactile Model-O and Teleoperation Framework Evaluation

The T-MO provides an adequate platform for initial experimentation in the use of TacTips for providing contact force information as well as bilateral teleoperation using the haptic feedback exoskeleton. However, a robot gripper with more DoFs could take full advantage of the complete finger poses calculated by the modified RF design.

Overall the teleoperation system works well and is effective at providing varying stiffness FF to the user during the grasping of different objects, as demonstrated in figure 4.6. The multithreaded approach to the software provides adequate processing speed, even when a large CNN is used to generate the force estimations. This allows the system to be responsive to rapid changes in contact force.

### 5.1.3 Force Estimation from Tactile Images Evaluation

The results shown in section 4.1.1 demonstrate that DL shows significant promise for estimating contact forces on TacTip tactile sensors. The use of CNNs provides more accurate estimations when compared to other approaches such as the use of SSIM. Furthermore, performance increases were observed when training CNNs using a training set containing tactile images from multiple sensors, showing the potential for this network architecture to generalise over different sensors, as long as their morphology is broadly the same. However, there are clear limitations to this approach in its current form. Notably, as seen in plot e of figure 4.1 the performance of force estimation using images from the middle sensor is noticeably worse than the other networks. This is not immediately apparent when looking at the MAE reported in table 4.1, however, the range of forces over which images were collected is significantly narrower for the middle sensor. This can be seen in the summary statistics shown in table 3.2. This is likely due to a hardware issue with the motor in the T-MO limiting the maximum force applied to the F/T sensor during data collection. A more thorough data collection process (such as directly attaching the TacTip to the end-effector of a robot arm) could solve this issue and allow the collection of a wider range of contact forces from a wider range of sensor poses. This would be more in line with the data collection process outlined in [14].

Further increases in DL performance could be obtained through hyperparameter optimisation (as demonstrated in [14]). The network architecture applied here was originally designed for pose estimation rather than contact force. Outside the scope of this project, optimising the network architecture could form the base of future work.

Another limitation of the DL approach is the predictions generated whilst undertaking teleoperation are lacking. It was found that querying a network trained on combined images would provide force estimations in only a small range, around 1N to 1.2N, despite a large variation in contact force and therefore sensor deformation. It is hypothesised that this is largely due to the limitations in the data collection procedure, particularly with the middle sensor. This could potentially be overcome by using a separate network for each sensor, however, this would require a significant increase in compute. Therefore, the force estimation using the image SSIM and a simple linear model was deployed for the teleoperation experiments. The estimation accuracy reduction is unfortunately a necessary trade-off in order to generate force estimations over the full range of forces recorded during the data collection. However, the use of SSIM allows much faster force estimation, increasing the response time of the system.

The use of SSIM for force inference itself stands to be improved. From figure 4.2, it can be seen that the data collected for the index and middle fingers does follow a roughly linear relationship, however, this is not seen in the thumb. Therefore a more complex linear model is likely to increase the performance of this approach, however, such an approach could be susceptible to overfitting.

## 5.2 Future Work

Hardware improvements could form the basis of future work. A number of improvements to the T-MO could be made, as outlined in section 3.1. There are also several possible improvements for the RF hardware. Firstly, RF could be re-extended to provide feedback to all five fingers, as done in the original design. However, this would require a significant rework of the electronics, such as the inclusion of a multiplexing circuit to handle the large number of analogue inputs for the three encoders per finger. Perhaps the most severe limitation in the RF design is the use of FSRs for force measuring. They have proved to be acceptable for certain applications but to improve the precision of the FF, another, more robust force measuring technology, such as a load cell could be used. This would, however, increase the weight, complexity and cost of the device. Another possible avenue is to investigate the use of tactile sensing in informing cutaneous haptics provided by a device such as TactiGrip [3]. Such a device could be easily added to RF and would likely improve the teleoperation experience dramatically.

Further evaluation of the system, including mounting the T-MO to a robot arm and performing more complex teleoperation tasks such as a box and blocks [11] task could be carried out. Such a setup would allow for the evaluation of the performance increase allowed by providing haptic feedback to a teleoperator. A comprehensive user study, with multiple participants, would

provide more detailed information on the experience of using RF and would likely result in the identification of more avenues for improvement of the hardware and software.

Remote Feelings has been identified as a strong candidate for use in VR. Integrating the device with an engine such as Unity would allow for highly controlled experiments in a wide variety of tasks without needing to deal with the complexities of real world use. This would also provide a platform for experimenting with different applications such as learning by demonstration, without the immediate need for more expensive and inaccessible hardware.

Contact force estimation using tactile sensors presents another direction for future work. Numerous potential improvements to the approach implemented here are outlined in 5.1, however, there is potential for novel techniques, not relying on DL to be explored. There is also potential for exploring the use of alternative tactile sensors, such as GelSight, for applications in teleoperation and haptics.

### 5.3 Conclusion

Considering the confluence of haptic feedback and tactile sensing, this project has explored the efficacy of using TacTip, optical tactile sensors to inform force feedback haptics provided by a modified version of the Remote Feelings haptic exoskeleton. This is done with a particular emphasis on accessibility and maintaining a low hardware cost with an aim of democratising research in an area that is characterised by expensive, hard-to-obtain hardware.

The RF design was heavily modified to extend its capabilities. Modifications include the addition of rotary encoders to the joints in the exoskeleton, allowing the calculation of the user's finger poses using forwards and inverse kinematics. The electronics were also simplified, with a move to the more accessible Arduino platform and the design of a PCB. These modifications result in a more capable FF exoskeleton whilst also reducing the cost even further than the original design. The performance of this device is assessed using free-motion, step-response and variable stiffness rendering experiments. It is found to perform well in these experiments, providing responsive and accurate feedback to the user.

Multiple techniques in estimating contact forces from tactile images have been explored. This includes the design of a data collection procedure, allowing the collection of many tactile images and the corresponding contact force information from a force/torque sensor. This data has been used to train numerous CNNs, exploring the impact on inference performance of different image processing techniques as well as combining data from different sensors. This assesses whether the DL approach is capable of generalising across different sensors, which typically require a unique model each. An alternative approach was explored, using SSIM to estimate the contact force. This measure has been previously applied to quantify the deformation of the soft surface of the sensors but not to directly infer the contact force. A strong relationship between SSIM and contact force is observed and a simple linear model provides a good approximation of the

contact force, however, further work is required to increase the accuracy for more demanding applications such as surgery.

A bilateral teleoperation framework was designed to allow the RF haptic exoskeleton to control the Tactile Model-O robotic gripper, equipped with three TacTip tactile sensors. The finger poses calculated by RF are used to individually control the fingers of the T-MO and the TacTips are used with the aforementioned force estimation techniques to provide contact force information to RF to allow accurate FF. This setup was tested in its ability to render the stiffnesses of different objects for a remote operator and was found to perform well at this task. Future work could explore the potential of this technology for more complex teleoperation, imitation learning and more advanced manipulation.

The key significance of this work is in the combination of the three main hardware components, the RF haptic exoskeleton, the T-MO and the TacTip tactile sensors. All three of these are constructed with primarily 3D printed and off-the-shelf components making them highly accessible and low-cost, especially when compared to other commercial offerings. Furthermore, estimating contact forces using TacTips is a novel use for these sensors, and, combined with their existing pose estimation abilities [14], they are shown to be highly versatile sensors capable of providing a large amount of useful contact information.

This work represents an exploration in utilising low-cost alternatives for conducting high impact research in tactile sensing, haptic feedback and teleoperation. Increasing the accessibility of research platforms for niche technologies can accelerate the rate of further development and allow more researchers from a variety of backgrounds to participate, diversifying and expanding the field.

## BIBLIOGRAPHY

- [1] *Senseglove*, 2023.  
<https://www.senseglove.com/>, last accessed: 21-02-2023.
- [2] A. C. ABAD AND A. RANASINGHE, *Visuotactile sensors with emphasis on gelsight sensor: A review*, IEEE Sensors Journal, 20 (2020), pp. 7628–7638.
- [3] G. E. BARNABY, *Breaking boundaries for adoption of accessible high fidelity haptic feedback technologies*, PhD thesis, The University of Bristol, 2022.
- [4] M. CAEIRO-RODRÍGUEZ, I. OTERO-GONZÁLEZ, F. A. MIKIC-FONTE, AND M. LLAMAS-NISTAL, *A systematic review of commercial smart gloves: Current status and applications*, Sensors, 21 (2021).
- [5] D. G. CALDWELL, L. ROZO, P. JIMÉNEZ, AND C. TORRAS, *A robot learning from demonstration framework to perform force-based manipulation tasks*, Intelligent Service Robotics, (2013).
- [6] X. GU, Y. ZHANG, W. SUN, Y. BIAN, D. ZHOU, AND P. O. KRISTENSSON, *Dexmo: An inexpensive and lightweight mechanical exoskeleton for motion capture and force feedback in vr*, CHI, (2016).
- [7] R. HINCET, V. VECHEV, H. SHEA, AND O. HILLIGES, *Dextres: Wearable haptic feedback for grasping in vr via a thin form-factor electrostatic brake*, UIST, (2018).
- [8] X. HU, A. WANG, AND A. CURTIS, *Remote feelings*, 2021.  
[https://github.com/BerkeleyCurtis/EECS249\\_HapticGlove](https://github.com/BerkeleyCurtis/EECS249_HapticGlove), last accessed: 14-11-2022.
- [9] J. W. JAMES, A. CHURCH, L. CRAMPHORN, AND N. F. LEPORA, *Tactile model o: Fabrication and testing of a 3d-printed, three-fingered tactile robot hand*, Soft Robotics, 8 (2021), pp. 594–610.
- [10] P. KORMUSHEV, S. CALINON, AND D. G. CALDWELL, *Imitation learning of positional and force skills demonstrated via kinesthetic teaching and haptic input*, Advanced Robotics, 25 (2011), pp. 581–603.

## BIBLIOGRAPHY

---

- [11] I. A. KULING, K. GIJSBERTSE, B. N. KROM, K. J. VAN TEEFFELEN, AND J. B. F. VAN ERP, *Haptic feedback in a teleoperated box & blocks task*, EuroHaptics, (2020).
- [12] M. LAMBETA, P.-W. CHOU, G. KAMMERER, D. JAYARAMAN, R. CALANDRA, B. MALOON, S. TIAN, V. R. MOST, B. YANG, R. SANTOS, AND A. BYAGOWI, *Digit: A novel design for a low-cost compact high-resolution tactile sensor with application to in-hand manipulation*, IEEE Robotics and Automation Letters, (2020).
- [13] N. F. LEPORA, *Soft biomimetic optical tactile sensing with the tactip: A review*, IEEE Sensors Journal, 21 (2021), pp. 21131–21143.
- [14] N. F. LEPORA AND J. LLOYD, *Optimal deep learning for robot touch: Training accurate pose models of 3d surfaces and edges*, IEEE Robotics & Automation Magazine, 27 (2020), pp. 66–77.
- [15] N. F. LEPORA, A. STINCHCOMBE, C. FORD, A. BROWN, J. W. LLOYD, M. G. CATALANO, M. BIANCHI, AND B. WARD-CHERRIER, *Towards integrated tactile sensorimotor control in anthropomorphic soft robotic hands*, 2021 IEEE International Conference on Robotics and Automation (ICRA), (2021).
- [16] M. LI, S. LUO, AND G. XU, *A tactile sensing and feedback system for tumor localization*, 2016 13th International Conference on Ubiquitous Robots and Ambient Intelligence (URAI), (2016).
- [17] W. LIN, B. WANG, G. PENG, Y. SHAN, H. HU, AND Z. YANG, *Skin-inspired piezoelectric tactile sensor array with crosstalk-free row+column electrodes for spatiotemporally distinguishing diverse stimuli*, Advanced Science, (2021).
- [18] R. MA AND A. DOLLAR, *Yale openhand project: Optimizing open-source hand designs for ease of fabrication and adoption*, IEEE Robotics & Automation Magazine, 24 (2017), pp. 32–40.
- [19] Z. MA AND P. BEN-TZVI, *Rml glove—an exoskeleton glove mechanism with haptics feedback*, IEEE-ASME Transactions on Mechatronics, (2015).
- [20] T. H. MASSIE, *The phantom haptic interface: A device for probing virtual objects*, null, (1994).
- [21] M. NETO, P. RIBEIRO, R. NUNES, L. JAMONE, A. BERNARDINO, P. P. FREITAS, AND S. CARDOSO, *A soft tactile sensor based on magnetics and hybrid flexible-rigid electronics*, Sensors, (2021).

- [22] L. U. ODHNER, L. P. JENTOFT, M. R. CLAFFEE, N. CORSON, Y. TENZER, R. R. MA, M. BUEHLER, R. KOHOUT, R. D. HOWE, AND A. M. DOLLAR, *A compliant, underactuated hand for robust manipulation*, The International Journal of Robotics Research, 33 (2014), pp. 736–752.
- [23] C. PACCHIEROTTI, D. PRATTICIZZO, AND K. J. KUCHENBECKER, *Cutaneous feedback of fingertip deformation and vibration for palpation in robotic surgery*, IEEE Transactions on Biomedical Engineering, (2016).
- [24] J. PARK, B. SON, I. HAN, AND W. LEE, *Effect of cutaneous feedback on the perception of virtual object weight during manipulation*, Scientific Reports, 10:1357 (2020).
- [25] A. PEER, S. EINENKEL, AND M. BUSS, *Multi-fingered telemanipulation - mapping of a human hand to a three finger gripper*, RO-MAN 2008 - The 17th IEEE International Symposium on Robot and Human Interactive Communication, (2008).
- [26] E. PSOMOPOULOU, N. PESTELL, F. PAPADOPoulos, J. W. LLOYD, Z. DOULGERI, N. F. LEPORA, AND N. F. LEPORA, *A robust controller for stable 3d pinching using tactile sensing*, arXiv: Robotics, (2021).
- [27] P. A. F. REZECK, B. FRADE, J. SOARES, L. PINTO, F. CADAR, H. AZPURUA, D. G. MACHARET, L. CHAIMOWICZ, G. M. FREITASS, AND M. F. M. CAMPOS, *Framework for haptic teleoperation of a remote robotic arm device*, 2018 Latin American Robotic Symposium, 2018 Brazilian Symposium on Robotics (SBR) and 2018 Workshop on Robotics in Education (WRE), (2018).
- [28] B. SICILIANO, L. SCIavicco, L. VILLANI, AND G. ORIOLO, *Robotics Modelling, Planning and Control*, Springer, 2009.
- [29] J. TIRADO, V. PANOV, V. YEM, D. TSETSERUKOU, AND H. KAJIMOTO, *Electroar: Distributed electro-tactile stimulation for tactile transfer*, in International Conference on Human Haptic Sensing and Touch Enabled Computer Applications, Springer, 2020, pp. 442–450.
- [30] T. P. TOMO, A. SCHMITZ, W. K. WONG, H. KRISTANTO, S. SOMLOR, J. HWANG, L. JAMONE, AND S. SUGANO, *Covering a robot fingertip with uskin: A soft electronic skin with distributed 3-axis force sensitive elements for robot hands*, IEEE Robotics and Automation Letters, (2018).
- [31] A. TOPINI, W. SANSOM, N. SECCIANI, L. BARTALUCCI, A. RIDOLFI, AND B. ALLOTTA, *Variable admittance control of a hand exoskeleton for virtual reality-based rehabilitation tasks*, Frontiers in Neurorobotics, 15 (2022).

## BIBLIOGRAPHY

---

- [32] M. L. TURNER, D. H. GOMEZ, M. R. TREMBLAY, AND M. R. CUTKOSKY, *Preliminary tests of an arm-grounded haptic feedback device in telemanipulation*, Dynamic Systems and Control, (1998).
- [33] L. VRTECH, *Lucidgloves*, 2021.  
<https://github.com/LucidVR/lucidgloves>, last accessed: 14-11-2022.
- [34] D. WANG, M. SONG, A. NAQASH, Y. ZHENG, W. XU, AND Y. ZHANG, *Toward whole-hand kinesthetic feedback: A survey of force feedback gloves*, IEEE Transactions on Haptics, (2019).
- [35] B. WARD-CHERRIER, L. CRAMPHORN, AND N. F. LEPORA, *Tactile manipulation with a tactuthumb integrated on the open-hand m2 gripper*, IEEE Robotics and Automation Letters, 1 (2016), pp. 169–175.
- [36] B. WARD-CHERRIER, N. PESTELL, L. CRAMPHORN, B. WINSTONE, M. E. GIANNACCINI, J. ROSSITER, AND N. F. LEPORA, *The tactip family: Soft optical tactile sensors with 3d-printed biomimetic morphologies*, Soft robotics, 5 (2018), pp. 216–227.
- [37] W. YUAN, S. DONG, AND E. H. ADELSON, *Gelsight: High-resolution robot tactile sensors for estimating geometry and force.*, Sensors, (2017).

## APPENDIX A

### Bill of Materials

The bill of materials (BOM) for the construction of the Remote Feelings haptic exoskeleton can be seen in table 1.

Part	Price /£	Quantity	Total Price /£	Links
TowerPro MG90s Servo Motor	2.99	3	8.99	1
FSR	6.81	3	20.43	2
Arduino Micro	18.98	1	18.98	3
PCB	5	1	5	4
10K Resistor	0.17	3	0.51	5
SV01 Rotary Encoder	0.81	6	4.86	6
Fingertip Holders	3.74	1	3.74	7
Velcro Strap	4.21	1	4.21	8
m2.5x16 Screw	0.04	4	0.16	9
m2x10 Screw	0.03	3	0.09	10
m2x6 Screw	0.32	3	0.96	11
m1.6x8 Screw	0.19	6	1.14	12
m3x4x6 Shoulder Screw	1.74	2	3.49	13
m3x4x16 Shoulder Screw	1.87	1	1.87	14
Torsion Spring	10.69	1	10.69	15
3D Printed Parts	4.50	1	4.50	16
Wires	3.29	1	3.29	17
		<b>TOTAL:</b>	£92.91	

Table 1: Table containing the bill of material for the construction of the modified Remote Feelings haptic exoskeleton described in this work.

# Faculty of Engineering Health and Safety: Risk Assessment Form

Name of Person Carrying Out Assessment: Christopher White

Title of Work: Using Tactile Sensing to Inform Low-Cost, Force-Feedback Haptics.

Risk Assessment Number Assigned (where applicable): [Click here to enter text.](#)

**Activity** (State: job, procedure, equipment, substances, hazard phrases, exposure, etc.)

**Brief Procedure:** Constructing a haptic feedback, exoskeletal glove using 3D printed parts and off-the-shelf electronic components. Then integrating this device with an underactuated robotic gripper equipped with tactile sensors. This will include soldering, use of 3D printers and use of low-powered electronics.

**Detailed Procedure:** Soldering components such as resistors and servo motors to a microcontroller. Constructing an exoskeleton out of 3D printed parts. Using this to control a robotic gripper actuated by more servo motors. Most of the time in the lab will just be computer-based work and coding.

<b>Location(s) of Activity:</b> <b>Bristol Robotics Lab</b>	<b>Activity owner:</b> Christopher White <b>Room Supervisor</b> (where appropriate): <a href="#">Click here to enter text.</a>
--	---

**Who will be doing the activity?** (State: competency level (any training required?), ability level (any accessibility issues/allergies where additional controls are needed? See page 4, section 7 for prompts)

Christopher White: Competent solderer and has completed H&S induction at BRL.

**Who else could be affected by the activity?** (e.g. other students in the vicinity, public)

Other academics/students with access to the lab. The lab is closed to the public and to most students.

Hazards Identified	Precautions to be taken
(refer to Hazard Identification list and note main hazards here, including chemical exposure limits etc. )	(Note protective clothing, safety screens, procedures, control, containment, venting, waste disposal, health monitoring etc.)
<b>1.</b> Soldering	<ul style="list-style-type: none"> <li>• Use proper equipment to hold hot soldering iron away from surfaces and body parts.</li> </ul>
<b>2.</b> Servos pushing/pulling fingers too far.	<ul style="list-style-type: none"> <li>• Use low-torque hobby servos and include hard limits in its positioning in the code controlling them.</li> <li>• Forces in the glove will be verified before any human use in order to ensure safe levels in all poses. This will ensure that no dangerous mechanical advantage has been created.</li> <li>• A Voltage controlled power source will be used to limit the maximum potential power.</li> </ul>

3. General hazards around the lab, including trips and potential falling objects from desks.	<ul style="list-style-type: none"> <li>• Standard procedures outlined in the BRL Health and Safety Induction.</li> </ul>
4.	<ul style="list-style-type: none"> <li>•</li> </ul>

**Services required.**

Water       Compressed Air       Compressed gases      Electrical Power

– 240V/13A       Other please specify \_\_\_\_\_

–3 Phase

**Emergency procedures in case of accident** (Note any special procedures, consider Human Factors page 4, section 7, also any hazards associated with loss of services ie power, air)

Fire: Evacuate to car park in front of lab.

Minor accidents reported using the UWE Health and Safety Accident Report Form.

**Special training requirements** (e.g. by advisor or another competent person, video, course etc.)
 

None

**Other Documents** (e.g. Manuals, Safety Data Sheets (SDS), procedure documents, etc. If any chemicals are used, a SDS must be provided)

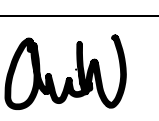
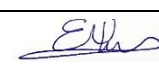
BRL Health and Safety Induction Presentation

**Access restrictions** (Note out-of-hours working rules, supervision requirements etc.)
 

BRL is open between 7am and 7pm Mon-Fri. Work will not be undertaken outside of these hours.

**Waste Disposal**

Any waste generated will be disposable as general waste.

	Name(s)	Status	Signature	Date
<b>All personnel involved in activity at the time of the assessment</b>	Christopher White	MEng student		27/10/22
<b>Advisor (competent member of staff)</b>	Efi Psomopoulou	Lecturer		16/11/2022
<b>Safety Advisor</b>		Choose an item.		

Technical Services <b>(If lab based)</b>	Andrew Stinchcombe	Technician	AJS	21/11/2022
---	--------------------	------------	-----	------------

At least 2 signatories required, 3 signatories preferred, if a laboratory or workshop-based activity then one of the signatories must be from Technical Services.

If carrying out this activity after the initial assessment has been completed, please sign the additional signature sheet at the end of this form.

---

**All Risk assessments must be reviewed at regular intervals or after a significant change/event.**

Issue Date: 27/10/2022

Review Due	Completed Date	Completed By:

# Health and Safety: Hazard Identification

The check list is guidance to help you but remember this does not cover all possible hazards.

<b>Location / Job – Final Year Project at BRL</b>	<b>Date: 27/10/2022</b>	
Name of Assessor: Christopher White		

<b>1. Mechanical Hazards</b>	<b>Yes</b>	<b>No</b>	<b>Hazard Description</b>
1.1. Crushing	<input type="checkbox"/>	<input checked="" type="checkbox"/>	
1.2. Cutting / shearing	<input type="checkbox"/>	<input checked="" type="checkbox"/>	
1.3. Entanglement	<input checked="" type="checkbox"/>	<input type="checkbox"/>	<b>Small hazard of servos pushing/pulling fingers too far.</b>
1.4. Drawing-in, trapping	<input type="checkbox"/>	<input checked="" type="checkbox"/>	
1.5. Impact	<input type="checkbox"/>	<input checked="" type="checkbox"/>	
1.6. Stabbing	<input type="checkbox"/>	<input checked="" type="checkbox"/>	
1.7. Slips, trips, falls	<input type="checkbox"/>	<input checked="" type="checkbox"/>	
1.8. Abrasion	<input type="checkbox"/>	<input checked="" type="checkbox"/>	
1.9. High pressure injection	<input type="checkbox"/>	<input checked="" type="checkbox"/>	
1.10. Other mechanical hazards	<input type="checkbox"/>	<input checked="" type="checkbox"/>	
<b>2. Electrical Hazards</b>	<b>Yes</b>	<b>No</b>	
2.1. Direct Contact	<input type="checkbox"/>	<input checked="" type="checkbox"/>	
2.2. Indirect Contact	<input type="checkbox"/>	<input checked="" type="checkbox"/>	
2.3. Short circuit / overload	<input type="checkbox"/>	<input checked="" type="checkbox"/>	
2.4. Source of ignition	<input type="checkbox"/>	<input checked="" type="checkbox"/>	
2.5. Other electrical hazards	<input type="checkbox"/>	<input checked="" type="checkbox"/>	
<b>3. Radiation Hazards</b>	<b>Yes</b>	<b>No</b>	
3.1. Lasers	<input type="checkbox"/>	<input checked="" type="checkbox"/>	
3.2. Ionising radiation	<input type="checkbox"/>	<input checked="" type="checkbox"/>	
3.3. Other electro-magnetic spectrum	<input type="checkbox"/>	<input checked="" type="checkbox"/>	
3.4. Other radiation hazards	<input type="checkbox"/>	<input checked="" type="checkbox"/>	
<b>4. Work practice Hazards</b>	<b>Yes</b>	<b>No</b>	
4.1. Highly repetitive actions	<input type="checkbox"/>	<input checked="" type="checkbox"/>	
4.2. Stressed postures	<input type="checkbox"/>	<input checked="" type="checkbox"/>	
4.3. Lifting / Handling	<input type="checkbox"/>	<input checked="" type="checkbox"/>	
4.4. Working at heights	<input type="checkbox"/>	<input checked="" type="checkbox"/>	
4.5. Visual fatigue	<input type="checkbox"/>	<input checked="" type="checkbox"/>	

4.6. Mental overload, stress		<input type="checkbox"/>	<input checked="" type="checkbox"/>	
4.7 Driving vehicles		<input type="checkbox"/>	<input checked="" type="checkbox"/>	
4.8 Working out of normal hours		<input type="checkbox"/>	<input checked="" type="checkbox"/>	
4.9 Lone working		<input type="checkbox"/>	<input checked="" type="checkbox"/>	
4.10 Other work practice hazards		<input type="checkbox"/>	<input checked="" type="checkbox"/>	
<b>5. Chemical risks (GHS hazard symbols)</b>		<b>Yes</b>	<b>No</b>	<b>List Hazard statements from Safety Data Sheets (SDS) where available</b>
5.1. Explosive chemicals GHS01		<input type="checkbox"/>	<input checked="" type="checkbox"/>	
5.2. Flammable chemicals GHS02		<input type="checkbox"/>	<input checked="" type="checkbox"/>	
5.3. Oxidisers - GHS03		<input type="checkbox"/>	<input checked="" type="checkbox"/>	
5.4. Pressurised gases - GHS04		<input type="checkbox"/>	<input checked="" type="checkbox"/>	
5.5. Corrosive chemicals - GHS05		<input type="checkbox"/>	<input checked="" type="checkbox"/>	
5.6. Acute Toxic chemicals – GHS06		<input type="checkbox"/>	<input checked="" type="checkbox"/>	
5.7. Health hazard (Irritants/sensitisers) - GHS07		<input type="checkbox"/>	<input checked="" type="checkbox"/>	
5.8. Serious Health hazard (Carcinogens/mutagens) - GHS08		<input type="checkbox"/>	<input checked="" type="checkbox"/>	
5.9. Ecological hazards - GHS09		<input type="checkbox"/>	<input checked="" type="checkbox"/>	
5.10. Biological hazards		<input type="checkbox"/>	<input checked="" type="checkbox"/>	
5.11. Other chemical hazards		<input type="checkbox"/>	<input checked="" type="checkbox"/>	
<b>6. Environmental Hazards</b>		<b>Yes</b>	<b>No</b>	
6.1. Localised hot surface(s)		<input type="checkbox"/>	<input checked="" type="checkbox"/>	
6.2. Localised cold surface(s)		<input type="checkbox"/>	<input checked="" type="checkbox"/>	
6.3. High ambient temperature		<input type="checkbox"/>	<input checked="" type="checkbox"/>	
6.4. Cold ambient temperature		<input type="checkbox"/>	<input checked="" type="checkbox"/>	

6.5. Poor ventilation	<input type="checkbox"/>	<input checked="" type="checkbox"/>	
6.6. Significant noise	<input type="checkbox"/>	<input checked="" type="checkbox"/>	
6.7 Significant vibration	<input type="checkbox"/>	<input checked="" type="checkbox"/>	
6.8 Poor lighting	<input type="checkbox"/>	<input checked="" type="checkbox"/>	
6.9 Working outside	<input type="checkbox"/>	<input checked="" type="checkbox"/>	
6.10 Other environmental hazards	<input type="checkbox"/>	<input checked="" type="checkbox"/>	
<b>7. Human Factor Considerations</b>	<b>Yes</b>	<b>No</b>	
7.1. Accessibility issues	<input type="checkbox"/>	<input checked="" type="checkbox"/>	
7.2. Allergies	<input type="checkbox"/>	<input checked="" type="checkbox"/>	
7.3. Autism	<input type="checkbox"/>	<input checked="" type="checkbox"/>	
7.4. Anxiety/Depression	<input type="checkbox"/>	<input checked="" type="checkbox"/>	
7.5. Dyslexia	<input type="checkbox"/>	<input checked="" type="checkbox"/>	
7.6. Deafness/Blindness	<input type="checkbox"/>	<input checked="" type="checkbox"/>	
7.7. Colour blindness	<input type="checkbox"/>	<input checked="" type="checkbox"/>	
7.8. Language barriers	<input type="checkbox"/>	<input checked="" type="checkbox"/>	
7.9. Age	<input type="checkbox"/>	<input checked="" type="checkbox"/>	
7.10. Behavioural issues	<input type="checkbox"/>	<input checked="" type="checkbox"/>	
7.11. New/expectant mothers	<input type="checkbox"/>	<input checked="" type="checkbox"/>	
7.11. Other medical conditions (skin conditions, respiratory problems etc.)	<input type="checkbox"/>	<input checked="" type="checkbox"/>	<i>Assess whether the activity would be more hazardous for those with certain medical conditions</i>
7.11. Other, please state	<input type="checkbox"/>	<input checked="" type="checkbox"/>	

# **Faculty of Engineering RISK ASSESSMENT**

## **ADDITIONAL SIGNATURE SHEET**

## **TITLE:** Using Tactile Sensing to Inform Low-Cost, Force-Feedback Haptics

## Risk Assessment Number:

*(If applicable)*

**THIS SIGNATURE SHEET ACCOMPANIES THE RISK ASSESSMENT REFERRED TO ABOVE.**

All workers involved in work covered by the risk assessment must sign below before commencing work. By signing below, you confirm that you have read the risk assessment and you agree to abide by the protocols and guidelines contained therein.

## Guidance for Writing Risk Assessments

Risk assessments should be about practical steps to protect people from real harm and suffering - not bureaucratic back covering. We need to establish that risk assessments are suitable and sufficient to ensure that:

- ❖ Staff, students and the public are properly protected
- ❖ innovation and learning are enabled not stifled
- ❖ those who create risks manage them responsibly
- ❖ individuals understand that as well as the right to protection, they also must exercise responsibility

### How to assess the risks in your work

Follow the six steps:

<b>Step 1</b>	List the work <b>tasks/activities</b>	Included the location of the work, activity planned, equipment and chemicals that may be in use
<b>Step 2</b>	Identify the <b>hazards</b>	Use the check list on the form to help you but remember this does not cover all hazards.
<b>Step 3</b>	Decide <b>who</b> might be harmed and how, so estimate the risks	Think about yourself, others around you, technicians, cleaners etc
<b>Step 4</b>	Evaluate the risks and decide on <b>precautions</b>	Be sensible - do you need signs to warn other people, protective equipment, work in a different location etc
<b>Step 5</b>	Record your findings and <b>implement</b> them	Use this form and follow the precautions you have identified as being required. Have a copy of this form in the location where you are working.
<b>Step 6</b>	<b>Review</b> your assessment and update if necessary	This should be done regularly or when you notice something is not working correctly

When thinking about your risk assessment, remember:

- ❖ a **hazard** is anything that may cause harm, such as chemicals, electricity, working from ladders/step stools, an open drawer etc;
- ❖ the **risk** is the chance, high or low, that somebody could be harmed by these and other hazards, together with an indication of how serious the harm could be.

$$\text{RISK} = \text{Likelihood} \times \text{Consequence}$$

### Additional information for chemical hazards - GHS Chemical hazard symbols

GHS01	GHS02	GHS03	GHS04	GHS05	GHS06	GHS07	GHS08	GHS09
								

Explosive   Flammable   Oxidising   Gas under pressure   Corrosive   Acute Toxicity   Health hazard   Serious health hazard   Hazardous to the environment

**This form must be completed electronically; no handwritten forms will be accepted as handwriting can make it difficult to understand information in an emergency.**

A copy of the final risk assessment should be available to you and others around you when you are working.

For off-site activities please follow the guidance available at <http://www.bristol.ac.uk/safety/guidance/#offsite>

And if necessary use the "Working off site risk assessment template" available on that webpage.